THE JOURNAL OF PHYSICAL CHEMISTRY B

ARTICLE

pubs.acs.org/JPCB

Universality in Self-Diffusion of Atoms among Distinctly Different Glass-Forming Liquids

Michio Tokuyama*

World Premier International Research Center, Advanced Institute for Materials Research and Institute of Fluid Science, Tohoku University, Sendai 980-8577, Japan

ABSTRACT: The long-time self-diffusion coefficients D_S^L in distinctly different glass-forming liquids are analyzed from a unified point of view recently proposed by the present author. It is shown that as long as the systems are in equilibrium, they are all described by the following two types of master curves, depending on whether the control parameter is intensive or extensive: $D_S^L(x) = d_0 x^{-1}(1-x)^{2+\eta}\exp[cx^{3+\eta}(1-x)^{2+\eta}]$ for a reduced intensive control parameter x, such as a reduced inverse temperature, and $D_S^L(x) = d_0 x^{-1}(1-x)^2$ for a reduced extensive control parameter x, such as a reduced volume fraction, where d_0 and c are constant. Here, the exponent η ($\neq 0$) results from many-body correlations in a supercooled liquid state. The constants η and c depend on the systems and are given by $(\eta,c) = (4/3,62)$ for fragile liquids, $(5/3, 62)$ for strong liquids, and $(0,0)$ for other glass-forming systems in which the peak heights of their non-Gaussian parameters are always much less than 1.0. It is also shown that all of the data for the diffusion coefficient start to deviate from the master curves at lower temperatures (or higher volume fraction), where the systems become out of equilibrium, leading to a glass state.

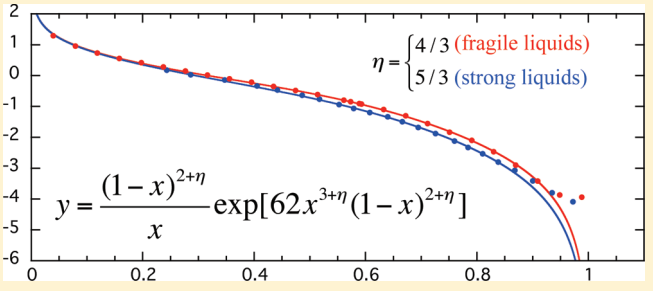

1. INTRODUCTION

The main purpose of the present paper is to analyze many experimental data and simulation results for self-diffusion in apparently different glass-forming liquids from a unified point of view recently proposed by the present author[1,2] consistently and thus to show that there exist quite marked universalities in their dynamics between very different glass transitions. In the present paper, we deal with three different types of systems separately, (F) fragile liquids, (S) strong liquids, and (O) other glass-forming systems, in which the peak heights of their non-Gaussian parameters $\alpha_2(t)$ are always much less than 1.0. As typical examples of (O), we here discuss hard spheres (HS) with 6% size polydispersity and solutions of mode-coupling theory (MCT) equations. Thus, we show that the diffusion data in those systems are well described by a single master curve as long as the systems are in equilibrium and start to deviate from it at lower temperatures (or higher volume fractions), where the systems become out of equilibrium, leading to a glass state.

As liquids are cooled below their melting points without crystallization, they become the so-called supercooled liquids.[3,4] Cooling them further below their glass transition temperatures T_g leads to glasses. Thus, there exist two different crossovers in viscous liquids upon cooling from high temperatures.[5−12] One is a crossover from an equilibrium liquid to an equilibrium-supercooled liquid. This is not any kind of phase transition from a liquid state to a supercooled state. The other is a gradual crossover from an equilibrium-supercooled liquid to a nonequilibrium glass. This is called the glass transition and is not a first-order phase transition. Some typical features in the dynamics of supercooled liquids are known to be quite different from those of liquids. First, in supercooled liquids, the nonlinear density fluctuations play an important role, and the many-body correlations crucially affect the dynamics. Hence, the relaxation function shows a nonexponential decay, and the peak height of the non-Gaussian parameter $\alpha_2(t)$ becomes higher than 1. On the other hand, in liquids, the linear density fluctuations play a role, and only the two-body correlations govern the dynamics, leading to an exponential decay and $\alpha_2(t) \ll 1$. Second, the transport properties such as the relaxation times and the viscosity exhibit extraordinary slow down close to T_g, while those are normal in liquids.

In the present paper, we focus only on the self-diffusion of atoms contained in distinctly different glass-forming liquids and mainly discuss the control parameter λ dependence of the long-time self-diffusion coefficient $D_S^L(\lambda)$. There are two types of control parameters. One is an intensive parameter, such as a temperature T and a pressure P. The other is an extensive parameter, such as a volume fraction ϕ and a specific volume V. As shown in the previous paper,[1] in a liquid state, the self-diffusion of any atom can be well described irrespective of the types of λ by a singular function

$$D_S^L(\lambda)/d_0 = (1-x)^2/x \tag{1}$$

where $x = \lambda/\lambda_c$ and the constant d_0 depend on the atom, λ_c being a fictive singular point whose value strongly depends on

Special Issue: H. Eugene Stanley Festschrift

Received: April 18, 2011
Revised: July 21, 2011
Published: August 11, 2011

the details of the systems. Because the function D_S^L/d_0 is independent of atom, the self-diffusion data for any atoms are collapsed onto it in a liquid state.[1,14] Here, the singular exponent 2.0 was originally obtained by calculating the long-time self-diffusion coefficient for a suspension of HS within the two-body correlations.[13] Hence, this is reasonable because only the two-body correlations play a role in the liquid state. In a supercooled state, however, the many-body correlations become important. Hence, all of the data would start to deviate from eq 1. As is shown in section 4, this is true for intensive parameters, while eq 1 still holds for extensive parameters. As discussed in the previous paper,[2] we assume that even in a supercooled state, the function D_S^L/d_0 still obeys a singular function of a reduced intensive parameter x as long as the system is in equilibrium and is given by

$$D_S^L(\lambda)/d_0 = (1-x)^{2+\eta}/x \tag{2}$$

where $x = \lambda/\lambda_f$, λ_f ($>\lambda_c$) being a new fictive singular point whose value strongly depends on the details of the systems. Here, the exponent η is assumed to result from the many-body correlations. The value of η is shown to depend on which types of systems the supercooled liquid belongs to, (F) $\eta = 4/3$, (S) 5/3, and (O) 0. Hence, we expect that all of the diffusion data are collapsed onto eq 2 near λ_f and start to deviate from it at higher values of λ, above which the system becomes out of equilibrium. By combining eqs 1 and 2, we thus show how to find a master function phenomenologically that describes the self-diffusion data in a whole region from a liquid state to a supercooled state as

$$D_S^L(x)/d_0 = x^{-1}(1-x)^{2+\eta}\exp[cx^{3+\eta}(1-x)^{2+\eta}] \tag{3}$$

where $x = \lambda/\lambda_f$ and c is constant. Here, eq 3 reduces to eq 1 for $x \ll 1$ and eq 2 for $x \approx 1$. By using this function, we also clarify the main mechanism to characterize a difference between fragile liquids and strong liquids. Thus, we discuss how one can describe similarities between different glass transition phenomena from a unified point of view consistently. We should note here that for extensive parameters λ, all of the diffusion data also start to deviate from eq 1 at higher values of λ, above which the system becomes out of equilibrium. Finally, we mention that when one analyzes the molecular dynamics simulation results by using eq 1 or eq 3, λ_f (or λ_c) is the only fitting parameter to be determined, while for analyses of experimental data and the embedded-atom method (EAM)-based simulation results, λ_f and d_0 are the only fitting parameters to be determined.

We begin in section 2 by briefly reviewing the mean-field theory (MFT) proposed by the present author.[15] In section 3, we show how one can extend MFT to describe a supercooled liquid and propose a master curve given by eq 3 as a function of an intensive parameter. In section 4, we show that there exist two types of master curves, depending on whether the control parameter is an extensive parameter or an intensive one. The extensive parameter dependence of the diffusion data is well described by the singular function eq 1, while the intensive parameter dependence is well described by the singular function eq 3. In section 5, we analyze the temperature dependence of self-diffusion data for fragile liquids, including viscous liquids, metallic melts, bulk waters, and confined water, and then show that all of the data are collapsed onto a single master curve given by eq 3 with $\eta = 4/3$. We also show that confined waters are well described by the master curve given by eq 1 even for an intensive parameter. In section 6, we analyze the temperature dependence of self-diffusion data for strong liquids and then show that all of the data are collapsed onto a single master curve given by eq 3 with $\eta = 5/3$. We also explore the main origin, which distinguishes strong liquids from fragile liquids. We conclude in section 7 with a summary.

2. MEAN-FIELD THEORY

In this section, we briefly summarize and discuss the basic equations and concepts obtained recently by MFT.[1,15]

A. Mean-Field Equation. We consider the multicomponent glass-forming $A_xB_yC_z\cdots$ liquids, which consists of N_α particles with mass m_α and diameter $\sigma_{\alpha\alpha}$, where $\alpha \in \{A,B,C,...\}$, $N = \sum_\alpha N_\alpha$ and $x + y + z + \cdots = 100$. We suppose that those systems undergo the glass transition as a control parameter λ increases, where λ is the control parameter, such as an inverse temperature $1/T$ and a volume fraction ϕ here. Let $\mathbf{X}_i^{(\alpha)}(t)$ denote a position vector of ith particle of atom α at time t. In this paper, we focus only on the dynamics of a single atom near the glass transition. The relevant variable to describe the slow relaxation of density fluctuations is then given by the self-intermediate scattering function

$$F_S^{(\alpha)}(q,t) = \langle \exp[i\boldsymbol{q}\cdot\{\mathbf{X}_i^{(\alpha)}(t) - \mathbf{X}_i^{(\alpha)}(t)\}]\rangle \tag{4}$$

where the brackets $\langle ...\rangle$ denote an equilibrium ensemble average and $\boldsymbol{q}$ is a wave vector. By employing the cumulant expansion method,[16] one can transform eq 4 into

$$F_S^{(\alpha)}(q,t) = \exp\left[-\frac{q^2}{6}M_2(t) + \frac{q^4}{2}\left(\frac{M_2(t)}{6}\right)^2\alpha_2(t) + O(q^6)\right] \tag{5}$$

with the non-Gaussian parameter[17]

$$\alpha_2(t) = \frac{3M_4(t)}{5M_2(t)^2} - 1 \tag{6}$$

where $M_2(t)$ and $M_4(t)$ are mean-square and mean-fourth displacements given by

$$M_n(t) = \langle|\mathbf{X}_i^{(\alpha)}(t) - \mathbf{X}_i^{(\alpha)}(0)|^n\rangle \tag{7}$$

The long-time self-diffusion coefficient D_S^L of atom α is then given by

$$D_S^L(\lambda) = \lim_{t\to\infty}\frac{M_2(t)}{6t} \tag{8}$$

In this paper, we discuss the λ dependence of D_S^L.

As shown by MFT,[15] the mean-square displacement $M_2(t)$ for molecular systems is described by the nonlinear mean-field equation

$$\frac{d}{dt}M_2(t) = 6D_S^L(\lambda) + 6[v_{th}^2 t - D_S^L(\lambda)]e^{-M_2(t)/\ell(\lambda)^2} \tag{9}$$

where the mean-free path $\ell(\lambda)$ is a length in which a particle can move freely without any interactions between particles and v_{th} ($=(k_BT/m_\alpha)^{1/2}$) is the thermal velocity. Although ℓ was originally related to the static structure factor $S(q)$,[18] it is determined by a fitting with data here. Equation 9 can be solve

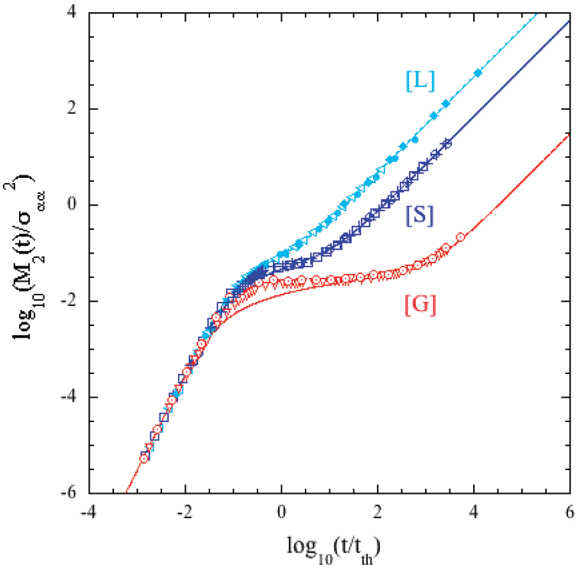

Figure 1. A log−log plot of $M_2(t)/\sigma_{\alpha\alpha}{}^2$ versus t/t_{th} for three different types of liquids, (F) a LJ binary mixture $A_{80}B_{20}$,[20] (S) SiO_2,[22] and (HS15%) a hard-sphere fluid with 15% size polydispersity.[23] The symbols indicate the simulation results: [L] $u = 2.11$, where (left-pointing open triangle) is the A particle at $T = 0.909$, (●) is O at $T = 0.227$, and (◇) is HS at $\phi = 0.54$; [S] $u = 2.93$, where (□) is A at $T = 0.588$, (+) is O at $T = 0.181$, and (○) is HS at $\phi = 0.57$; and [G] $u = 5.3$, where (⊙) is A at $T = 0.417$ and (▽) is HS at $\phi = 0.6$. The solid lines indicate the mean-field solutions given by eq 10, where $\ell/\sigma_{\alpha\alpha} = 0.113$ [L], 0.0856 [S], and 0.043 [G].

to give a formal solution

$$M_2(t) = 6D_S^L t + \ell^2 \ln\left[e^{-6t/t_\beta} + \frac{1}{6}\left(\frac{t_\beta}{t_f}\right)^2\{1 - (1 + 6t/t_\beta)e^{-6t/t_\beta}\}\right] \quad (10)$$

where t_β $(=\ell^2/D_S^L)$ denotes a time for a particle to diffuse over a distance of order ℓ with the diffusion coefficient D_S^L and is identical to the so-called β-relaxation time. Here, t_f $(=\ell/v_{th})$ is a mean-free time, within which each particle can move freely without any interactions between particles.

Because ℓ is uniquely determined by D_S^L,[19] the mean-field solution (eq 10) suggests that the dynamics of $M_2(t)$ is determined by only one parameter

$$u = \log_{10}(\sigma_{\alpha\alpha}v_0/D_S^L) \quad (11)$$

where v_0 $(=\varepsilon_{\alpha\alpha}/m_\alpha)^{1/2}$ is a particle average velocity, $\varepsilon_{\alpha\alpha}$ being an energy. Depending on the values of u, there are three different states, a liquid state [L] for $u < u_\beta$, a supercooled state [S] for $u_\beta \le u < u_g$, and a glass state [G] for $u_g \le u$, where $u_\beta \simeq 2.6$ and $u_g \simeq 5.1$.[19] If u has the same value in different systems, the dynamics in different systems becomes identical to each other. We call this a universality in dynamics (UI). In Figure 1, a log−log plot of $M_2(t)$ is shown versus t/t_{th} at the same value of u for three different types of liquids, F liquids with $\lambda = 1/T$, S liquids with $1/T$, and HS liquids with ϕ, where $t_{th} = \sigma_{\alpha\alpha}/v_{th}$. Examples are given by (F) Lennard-Jones (LJ) binary mixture $A_{80}B_{20}$,[20] (S) SiO_2,[22] and (HS15%) hard-sphere fluid with 15% size polydispersity.[23] As discussed in the previous paper,[1] the MFT is valid only for $u < u_x$ ($\simeq$3.04), except HS where MFT holds in both states [L] and [S]. Hence, in each state shown in Figure 1, [L] at $u = 2.11$ and [S] at $u = 2.93$, all the results for three types of liquids are shown to be collapsed onto the master curve given by eq 10, showing UI. However, we should note that the UI still holds even in a deeply supercooled state for $u_g > u > u_x$, although MFT no longer exists there. On the other hand, in a glass state, the simulation results do not agree with each other in the β stage for $t_f < t \le t_\beta$ because the liquids are out of equilibrium.

Table 1. Potentials and $\kappa_{\alpha\alpha}$

atom	potential [ref]	$\kappa_{\alpha\alpha}$
Ni in $Ni_{80}P_{20}$	Stillinger−Weber (SW)[24]	12
P in $Ni_{80}P_{20}$	SW[24]	6
A in $A_{80}B_{20}$	Lennard-Jones (LJ)[25]	48
B in $A_{80}B_{20}$	LJ[25]	24
O in SiO_2	Nakano−Vashishta (NV)[26]	15.31
Si in SiO_2	NV[26]	27.35
Cu in $Cu_{60}Ti_{20}Zr_{20}$	Han−Teichler (HT)[27]	9
Ti in $Cu_{60}Ti_{20}Zr_{20}$	HT[27]	4
Zr in $Cu_{60}Ti_{20}Zr_{20}$	HT[27]	3
hard spheres	step function ($n_{\alpha\alpha} = \infty$)[1]	1

B. Long-Time Self-Diffusion Coefficient. In a liquid state, the long-time self-diffusion coefficient $D_S^L(\lambda)$ for the molecular systems is described by a singular function[1,14]

$$\frac{D_S^L(\lambda)}{\sigma_{\alpha\alpha}v_0} = \kappa_{\alpha\alpha}^{-1}\left(\frac{\lambda_c}{\lambda}\right)\left(1 - \frac{\lambda}{\lambda_c}\right)^2 \quad (12)$$

with the coefficient

$$\kappa_{\alpha\alpha} = \frac{\sigma_{\alpha\alpha}}{\varepsilon_{\alpha\alpha}}\left(-\frac{\partial U_{\alpha\alpha}^{rep}(r)}{\partial r}\right)\Bigg|_{r=\sigma_{\alpha\alpha}} \quad \text{for } \lambda = 1/T \quad (13)$$

and

$$\kappa_{\alpha\alpha} = \frac{1}{\varepsilon_{\alpha\alpha}\sigma_{\alpha\alpha}^3}\int_{\sigma_{\alpha\alpha}}^{\infty} dr\, r^3\left(-\frac{\partial U_{\alpha\alpha}^{rep}(r)}{\partial r}\right) \quad \text{for } \lambda = \phi \quad (14)$$

where λ_c is a fictive singular point to be determined by fitting eq 12 with data. Here, $U_{\alpha\beta}^{rep}(r)$ is a repulsive part of a pair potential $U_{\alpha\beta}(r)$. If one takes $U_{\alpha\beta}^{rep}(r) = \varepsilon_{\alpha\beta}(\sigma_{\alpha\beta}/r)^{n_{\alpha\beta}}$, one then obtains $\kappa_{\alpha\alpha} = n_{\alpha\alpha}$ for $\lambda = 1/T$ and $\kappa_{\alpha\alpha} = n_{\alpha\alpha}/(n_{\alpha\alpha} - 3)$ for $\lambda = \phi$, where $n_{\alpha\beta}$ is a positive constant. Here, we note that the coefficient $\kappa_{\alpha\alpha}$ describes the characteristic feature of atom α. Hence, it has the same value for atom α even if it belongs to any multicomponent systems.[14] Typical examples of the potentials and the calculated value of $\kappa_{\alpha\alpha}$ are listed in Table 1. Near λ_c, one can also write eq 12 as

$$D_S^L(\lambda) \approx \epsilon^2 \quad (15)$$

where $\epsilon = 1 - \lambda/\lambda_c$ (≥ 0).

In Figure 2, a log plot of $D_S^L/\sigma_{\alpha\alpha}v_0$ is shown versus λ/λ_c for four different types of liquids, (F) the LJ binary mixture $A_{80}B_{20}$ with $1/T$, (S) SiO_2 with $1/T$, (HS15%) hard-sphere fluid with 15% size polydispersity with ϕ, and (MCT) solutions of mode-coupling theory equations for quasi-hard spheres with ϕ at $n_{\alpha\alpha} = 36$ and 10% size polydispersity[28] and those for the LJ binary colloids $A_{80}B_{20}$ with $1/T$.[29] The simulation results in (F) and (S) start to deviate from the mean-field curve given by eq 12 around u_x because λ is an intensive parameter, while

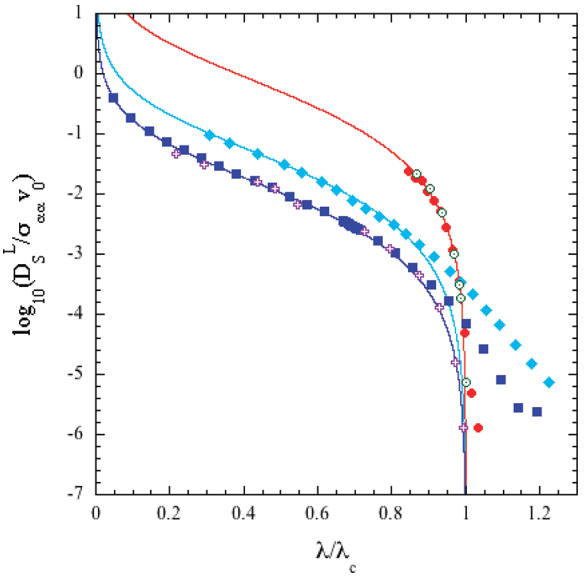

Figure 2. A log plot of $D_S^L/\sigma_{\alpha\alpha}v_0$ versus λ/λ_c for four different types of liquids, (F) a LJ binary mixture $A_{80}B_{20}$,[20] (S) SiO_2,[22] (HS15%) a hard-sphere fluid with 15% size polydispersity,[23] and (MCT) a quasi-hard-sphere system[28] and LJ binary colloids $A_{80}B_{20}$.[29] The symbols indicate the simulation results, (□) A atom, (◇) O, (○) hard spheres, (⊙) quasi-hard spheres, and (+) A colloid. The solid lines indicate the mean-field results given by eq 11, where T_c, ϕ_c, and $\kappa_{\alpha\alpha}$ are listed in Table 2.

Table 2. T_c, ϕ_c, $\kappa_{\alpha\alpha}$, and D_S^S

system [ref]	symbol	λ_c	$\kappa_{\alpha\alpha}$	simulation	D_S^S
(F) fragile liquids					
A in LJ mixture[20]	(□)	$T_c = 0.476$	48	MD	–
(S) strong liquids:					
O in SiO_2[22]	(◇)	$T_c = 0.168$	15.31	MD	–
(HS) hard spheres:					
15% size polydispersity[23]	(○)	$\phi_c = 0.591$	1.0	MD	–
(MCT) MCT solutions:					
quasi-hard spheres[28]	(⊙)	$\phi_c = 0.514$	36/33	MD	–
A in LJ colloids[29]	(+)	$T_c = 0.955$	48	BD	0.24

those in (HS15%) still obey eq 12 because λ is an extensive parameter, and they finally start to deviate from the mean-field curve around u_g, below which the liquids become out of equilibrium. On the other hand, the simulation results in (MCT) always obey eq 12 irrespective of the types of λ. This is because in (MCT), only the two-body correlations are taken into account. Here, we should also note that the MCT solutions for LJ colloids do not agree with the MD results for LJ mixtures at higher temperatures because the colloids are described by the long-time self-diffusion coefficient different from eq 12 as[15]

$$\frac{D_S^L(\lambda)}{D_0} = \frac{D_S^S/D_0}{1 + \kappa_{\alpha\alpha}(D_S^S/D_0)(\lambda/\lambda_c)(1-\lambda/\lambda_c)^{-2}} \tag{16}$$

where $D_S^S(\phi)$ is a short-time self-diffusion coefficient (see refs 13 and 30 for details) and D_0 a single-particle diffusion

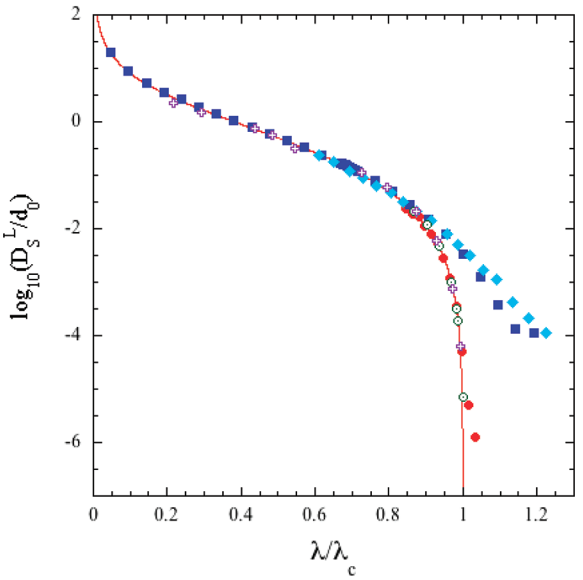

Figure 3. A log plot of D_S^L/d_0 versus λ/λ_c for four different systems, (F) LJ binary mixture $A_{80}B_{20}$,[20] (S) SiO_2,[22] (HS15%) hard-sphere fluid with 15% size polydispersity,[23] and (M) quasi-hard spheres[28] and LJ binary colloids $A_{80}B_{20}$.[29] The details are the same as those in Figure 2.

constant. Hence, eq 16 has the asymptotic forms

$$\frac{D_S^L(\lambda)}{D_0} \simeq \begin{cases} (D_S^S(\phi)/D_0)[1 - \kappa_{\alpha\alpha}(D_S^S/D_0)x] & \text{for} \quad x \ll 1 \\ \kappa_{\alpha\alpha}^{-1}(1-x)^2/x & \text{for} \quad x \geq 0.4 \end{cases} \tag{17}$$

where $x = \lambda/\lambda_c$. Thus, the colloids are described by the same equation as eq 12 for $x \geq 0.4$, while they do not obey eq 12 for $x \ll 1$. In fact, this is seen in Figure 2.

The difference between the simulation results in a liquid state [L] is only due to $\kappa_{\alpha\alpha}$. In order to eliminate such a difference, it is convenient to introduce a new variable d_0 by

$$d_0 = \sigma_{\alpha\alpha}v_0/\kappa_{\alpha\alpha} \tag{18}$$

Then, eq 12 suggests that in [L], all of the simulation results for D_S^L/d_0 collapse onto a single master curve given by eq 12.[31] In fact, this is seen in Figure 3. However, in a supercooled state [S], the simulation results in (F) and (S) start to deviate from eq 12 and do not coincide with each other. On the other hand, those in (HS15%) obey eq 12 even in [S] and finally start to deviate from it in [G]. This apparent behavior is just because λ is a volume fraction. In fact, in section 4, the hard-sphere fluid with 15% size polydispersity is shown to be one of fragile liquids because the peak height of the non-Gaussian parameter $\alpha_2(t)$ becomes larger than 1.0 in [S]. Thus, we emphasize that even in [S], all of the results except in (O) should collapse onto a single master curve just as in [L]. In fact, in the next section, we discuss such a new mater curve onto which all of the data collapse both in [L] and [S]. We call this a universality in D_S^L (UII).

C. α- and β-Relaxation Times. We now discuss the D_S^L dependence of α- and β-relaxation times, t_α and t_β, respectively. As discussed above, the dynamics in different systems are identical to each other if the value of u is the same. Hence, both times t_α and t_β are also determined by D_S^L only. Here, t_β is a time scale on which the particles can escape from their cages. On a time scale shorter than it, each particle behaves as if it is trapped

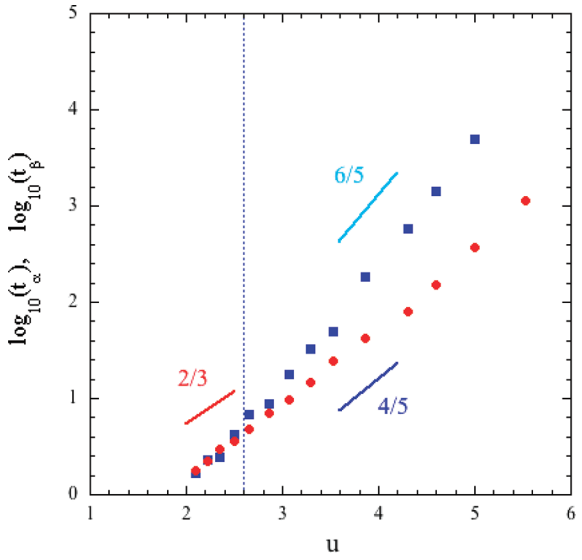

Figure 4. A log plot of t_α and t_β versus u for the LJ binary mixture $A_{80}B_{20}$. The symbols indicate the simulation results from ref 20, (□) t_α for A particle and (○) t_β for A particle. The solid lines indicate slopes of around 2/3, 4/5, and 6/5. The vertical dotted line indicates the supercooled point u_β (≃2.6). Here, the vertical scales are adjusted so that t_α coincides with t_β in a liquid state.

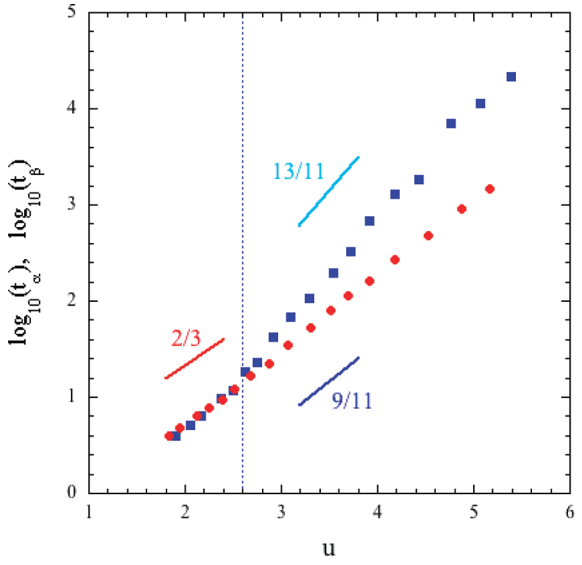

Figure 5. A log plot of t_α and t_β versus u for SiO_2. The symbols indicate the simulation results from ref 22, (□) t_α for O and (○) t_β for O. The solid lines indicate slopes of around 2/3, 9/11, and 13/11. The details are the same as those in Figure 4.

in a cage, which is mostly formed by neighboring particles. The α-relaxation time t_α is defined as a time on which the self-intermediate scattering function $F_S(q,t)$ decays to e^{-1} of its initial value, that is, $F_S(q,t_\alpha) = e^{-1}$.

In the following, we investigate how those relaxation times show a power law dependence on D_S^L in four different types of liquids, (F), (S), (HS), and (MCT). In Figure 4, the relaxation times t_α and t_β of A particle in the LJ binary mixture $A_{80}B_{20}$ are shown versus u as a typical example of (F). In a liquid state [L]

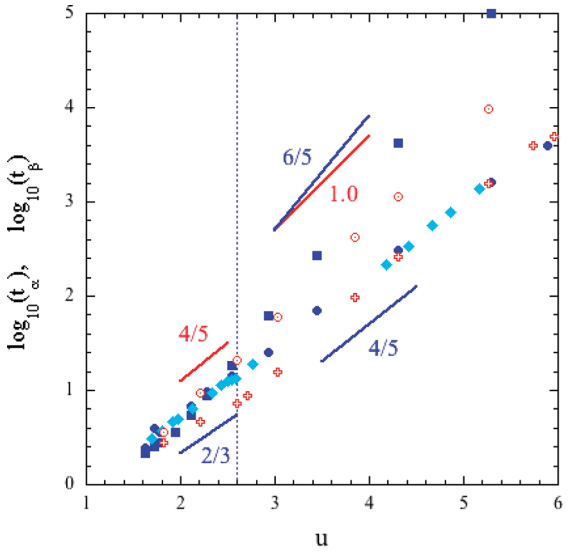

Figure 6. (A log plot of t_α and t_β versus u for hard spheres in different systems. The symbols indicate the simulation results for hard spheres from ref 23, (□) t_α with 15% size polydispersity, (●) t_β with 15% size polydispersity, and (◇) t_β with 6% size polydispersity. The other symbols indicate the experimental data for colloids with 6% size polydispersity from ref 32, (⊙) t_α and (+) t_β. The solid lines indicate slopes of around 2/3, 4/5, 1.0, and 6/5. The details are the same as in Figure 4.

for $u < u_\beta$, those seem to obey the same power law with an exponent around 2/3, while in a supercooled state [S] for $u_\beta \le u < u_g$, t_α has an exponent around 6/5 and t_β around 4/5. Thus, the exponent is different in both states. This crossover suggests that in [S], the many-body correlations play an important role in self-diffusion of a single atom, while in [L], only the two-body correlations do. Such a crossover is also seen in the peak time of the non-Gaussian parameter $\alpha_2(t)$,[21] where its peak height becomes larger than 1.0 in [S], while it is less than 1.0 in [L]. In Figure 5, t_α and t_β of O in SiO_2 are shown versus u as an example of (S). The situation is very similar to that in fragile liquids, although the values of the power law exponents in [S] are slightly different from those of (F). In Figure 6, t_α and t_β of hard spheres with 6 and 15% size polydispersities are also shown versus u as an example of (HS). In both states [L] and [S] for hard spheres with 6% size polydispersity, there exists no crossover where t_α and t_β have exponents of 1.0 and 4/5, respectively. This situation is quite different from that in (F) and (S). This means that only the two-body correlations play a role in [L] and [S]. In fact, the peak height of $\alpha_2(t)$ is always less than 1.0. On the other hand, for hard spheres with 15% size polydispersity, t_α has an exponent of 2/3 in [L] and 6/5 in [S], while t_β has 2/3 in [L] and 4/5 in [S]. The peak height of $\alpha_2(t)$ becomes larger than 1.0 in [S]. Hence, this situation is exactly the same as that in (F). We discuss this in section 4. Finally, in Figure 7, t_α and t_β obtained by the MCT solutions in two different systems are shown versus u. One is the quasi-hard spheres with $n_{\alpha\alpha} = 36$ and 10% size polydispersity,[28] and another is the LJ binary colloids $A_{80}B_{20}$.[29] In both states [L] and [S], there exists no crossover where t_α and t_β have exponents of 1.0 and 4/5, respectively. This situation is exactly the same as that in hard spheres with 6% size polydispersity.

For all four different types of liquids, (F), (S), (HS), and (MCT), both relaxation times t_α and t_β show a power law

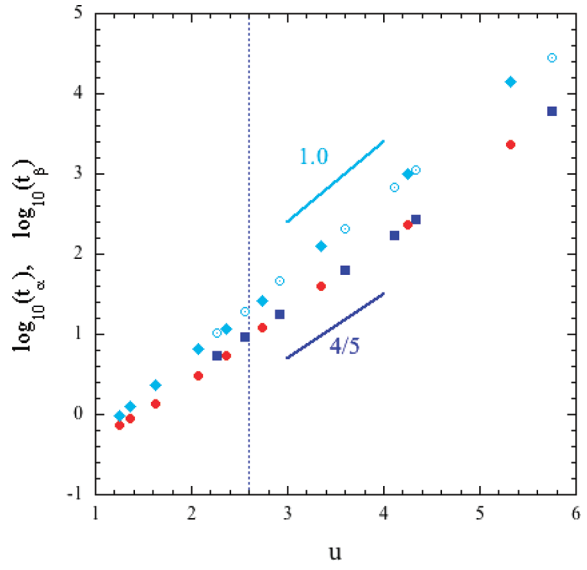

Figure 7. A log plot of t_α and t_β versus u for MCT solutions in two different systems, the quasi-hard spheres[28] and the LJ binary colloids $A_{80}B_{20}$.[29] The symbols indicate the MCT results for A particle (◇) t_α and (○) t_β and for hard spheres (⊙) t_α and (□) t_β. The solid lines indicate slopes of around 4/5 and 1.0. The details are the same as those in Figure 4.

behavior. In a liquid state [L], they obey the power laws as

$$t_\alpha \approx (D_S^L)^{-(1-\nu_\alpha)} \qquad t_\beta \approx (D_S^L)^{-(1-\nu_\beta)} \tag{19}$$

where ν_i is an exponent to be determined. In a supercooled state [S], they also obey the power laws as

$$t_\alpha \approx (D_S^L)^{-(1-\mu_\alpha)} \qquad t_\beta \approx (D_S^L)^{-(1-\mu_\beta)} \tag{20}$$

where μ_i is an exponent to be determined. The exponents μ_i and ν_i are listed in Table 3. Here, we note that the power law exponents μ_i are related to the many-body correlations, while ν_i is related to the two-body correlations. If $|\mu_i| = |\nu_i|$, however, only the two-body correlations play an role in self-diffusion. (O) belongs to this case. The slight difference between the value of μ_α in (F) and that in (S) might be mainly caused by the fact that the interactions between atoms in (S) have a long-range nature, while those in (F) a short-range nature. This will be confirmed in section 6 by comparing the simulation results on SiO_2 with three-body interactions with those without such interactions. We also note that for the systems with $\mu_\alpha \neq 0$, the peak height of $\alpha_2(t)$ always becomes larger than 1.0 in a supercooled state [S]. For the systems with $\mu_\beta \neq \nu_\beta$, the MFT does not hold in [S]. On the other hand, for the systems with $\mu_\beta = \nu_\beta$, the MFT holds in both states [L] and [S]. Finally, we should mention that the features of the MCT solutions are exactly the same as those in hard spheres with size polydispersities less than 10%, where the peak height of $\alpha_2(t)$ is always less than 1.0 in both states [L] and [S]. Next, we discuss how one can extend eq 12 to describe a supercooled liquid from a unified point of view based on the power law behavior of t_α and t_β shown in eqs 19 and 20.

3. SELF-DIFFUSION IN SUPERCOOLED LIQUIDS

In this section, we discuss the intensive parameter dependence of the long-time self-diffusion coefficient D_S^L in a supercooled state. This is because, as shown in the next section, the extensive

Table 3. μ_α, ν_α, μ_β, ν_β, η, and γ, where $\eta = 2(\nu_\beta/\mu_\beta - 1)$ and $\gamma = 2 + \eta = 2\nu_\beta/\mu_\beta$

system	μ_α	ν_α	μ_β	ν_β	η	γ
(F) fragile liquids: LJ binary mixture HS 15%	−1/5	1/3	1/5	1/3	4/3	10/3
(S) strong liquids: SiO_2	−2/11	1/3	2/11	1/3	5/3	11/3
(O) others with $\alpha_2(t) \ll 1$: HS 6% MCT solutions	0	0	1/5	1/5	0	2

parameter dependence of the diffusion data is completely described by the singular function given by eq 12. As discussed in the previous section, in a supercooled state, eq 12 is no longer valid because the many-body correlations become important, where $\alpha_2(t) \geq 1.0$.[1] However, we assume that even in [S], the same singular function as eq 12 still holds as long as the liquids are in equilibrium, except that the exponent 2.0 is now replaced by the renormalized one. Thus, we have[2]

$$\frac{D_S^L(\lambda)}{\sigma_{\alpha\alpha}\nu_0} = \kappa_{\alpha\alpha}^{-1}\left(\frac{\lambda_f}{\lambda}\right)\left(1 - \frac{\lambda}{\lambda_f}\right)^{2+\eta} \tag{21}$$

where λ_f ($>\lambda_c$) is a new fictive singular point to be determined and η an exponent related to the many-body correlation effects. Near λ_f, one also finds

$$D_S^L(\lambda) \approx \epsilon^\gamma \tag{22}$$

where $\epsilon = 1 - \lambda/\lambda_f\ (\geq 0)$ and $\gamma = 2 + \eta$. Similarly to λ_c, the value of λ_f is obtained by fitting. Next, we show how to calculate the value of η approximately. In order to calculate the exponent η, one may use the power law behavior of t_β.[2] Because $t_\beta = \ell_\beta^2/D_S^L$, use of eqs 19, 20, and 22 then leads to

$$\ell_\beta \approx \epsilon^{\nu_\beta} \qquad \text{in [L]} \tag{23}$$

$$\ell_\beta \approx \epsilon^{(2+\eta)\mu_\beta/2} \qquad \text{in [S]} \tag{24}$$

In both states [L] and [S], the mean-free path ℓ_β decreases as λ increases. Because the mechanism of a caging does not change in both states, the power law exponent of ℓ_β should be the same in both states. Use of eqs 23 and 24 then leads to

$$2\nu_\beta = (2 + \eta)\mu_\beta \qquad \text{or } \eta = 2(\nu_\beta/\mu_\beta - 1) \tag{25}$$

Here, the value of η depends on the system and is listed in Table 3. In [S], we also find

$$\gamma = 2 + \eta = 2\nu_\beta/\mu_\beta \tag{26}$$

while eq 15 holds in [L] for any type of liquids.

The long-time self-diffusion coefficient D_S^L is described by eq 12 in a liquid state [L], while it is described by eq 21 in a supercooled state [S]. In order to find an asymptotic function of D_S^L that describes a whole self-diffusion process from a liquid to a supercooled liquid, we assume that D_S^L can be written as

$$D_S^L/d_0 = f(\lambda/\lambda_f) \tag{27}$$

where $f(x)$ is a function of x to be determined and d_0 is given by eq 18. Then, the function $f(x)$ must reduce to eq 21 in [S] and

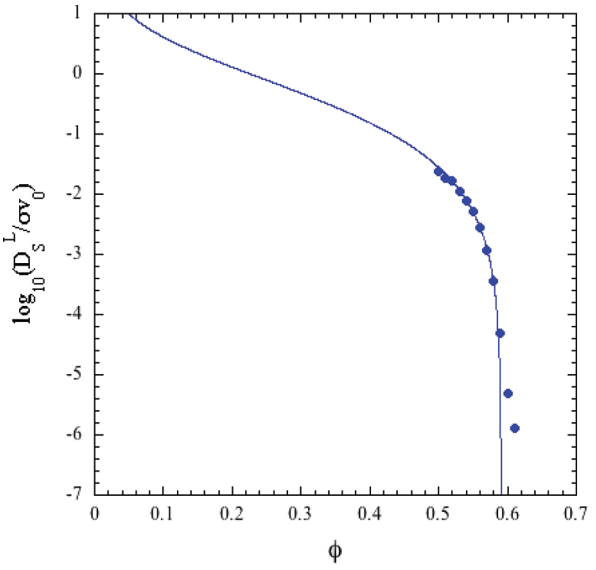

Figure 8. A log plot of D_S^L for hard spheres with 15% size polydispersity versus ϕ. The symbols indicate the simulation results from ref 23. The solid line indicates the singular function given by eq 12, where $\kappa = 1.0$ is a theoretical value for HS and $\phi_c = 0.5908$ is a fitting value.

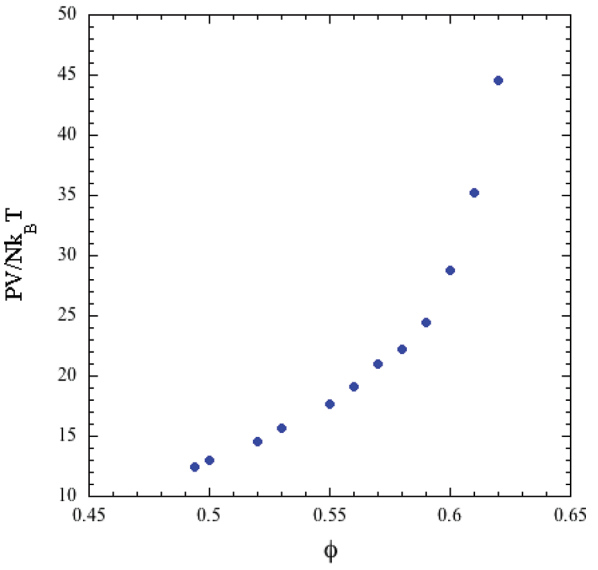

Figure 9. A plot of P for the simulation results on hard spheres with 15% size polydispersity versus ϕ. The symbols indicate the simulation results from ref 23.

eq 12 in [L]. In order to find such a function, therefore, one may expand it in powers of ϵ^γ/x as

$$f(x) = \frac{\epsilon^\gamma}{x}\left[1 + g_1(x)\frac{\epsilon^\gamma}{x} + \quad \ldots \quad\right] \tag{28}$$

where $g_1(x)$ is a function of x to be determined. Equation 28 must satisfy the conditions that $f(x) \approx x^{-1}$ for $x \ll 1$ and $f(x) \approx \epsilon^\gamma$ for $x \approx 1$. Hence, one finds $g_1(x) \sim cx^b$, where b and c are positive constants. Here, b and c are determined so that $f(x)$ satisfies eq 15 for intermediate values of x. Thus, we find $c \simeq 62$ and $b \simeq 4 + \eta$. Then, use of eq 28 leads to

$$\begin{aligned} f(x) &= \frac{\epsilon^\gamma}{x}\left[1 + cx^{4+\eta}\frac{\epsilon^\gamma}{x} + \quad \ldots \quad\right] \\ &\simeq \frac{(1-x)^{2+\eta}}{x}\exp\left[cx^{4+\eta}\frac{(1-x)^{2+\eta}}{x}\right] \end{aligned} \tag{29}$$

Equation 29 is an asymptotic function that describes a whole diffusion process from a liquid state to a supercooled state. In the next sections, this function is tested by analyzing many different simulation results and experimental data as a function of the intensive control parameter. Thus, we show that any self-diffusion data collapse onto this singular function as a master curve as long as the systems are in equilibrium.

4. INTENSIVE PARAMETER DEPENDENCE OF D_S^L AND THE EXTENSIVE ONE

In this section, we discuss why the volume fraction dependence of the long-time self-diffusion coefficient for hard spheres with 15% size polydispersity is well described by the singular function eq 12 but not by eq 27 with $\eta \neq 0$ and also clarify whether it is consistent with the following facts: (1) the peak height of $\alpha_2(t)$ becomes larger than 1.0 in [S] and (2) the relaxation times show the same power law behavior as that in fragile liquids, that is, $\eta = 4/3$. Those

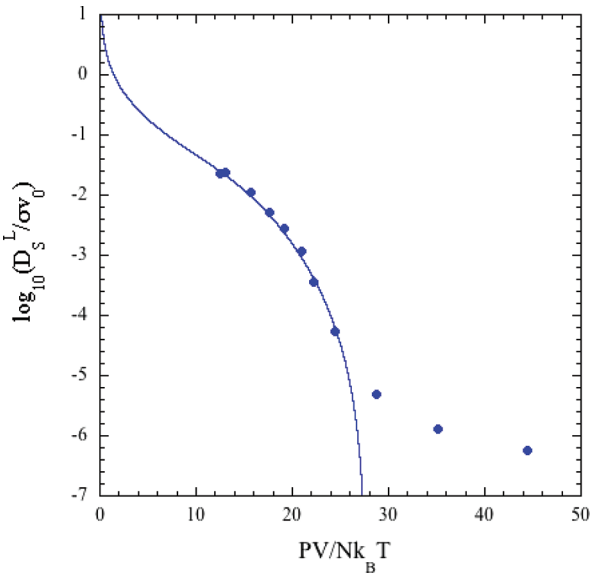

Figure 10. A log plot of D_S^L versus PV/Nk_BT. The symbols indicate the simulation results from ref 23. The solid line indicates the singular function given by eq 27 with $\eta = 4/3$, where $\kappa = 16$ is a fitting value and $P_f = 27.8k_BT/V$ is a fitting value.

results all depend on whether the control parameter λ is intensive or extensive. As simple examples, we analyze two different molecular dynamics simulation results. One is the molecular dynamics simulation results on the hard-spheres with 15% size polydispersity[23] performed by the so-called *NVT* method, where the control parameter is the volume fraction ϕ. The other is the molecular dynamics simulation results on pentane with the Lennard-Jones potential[33] performed by the so-called *NPT* method, where the control parameter is an inverse temperature.

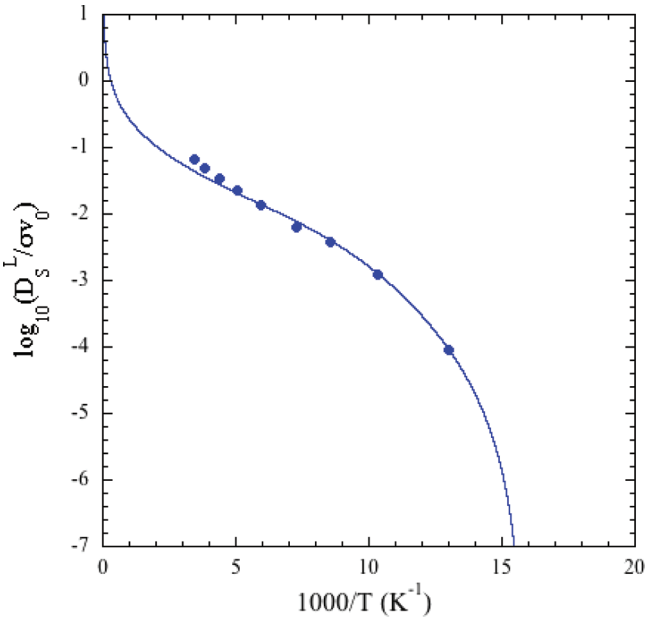

Figure 11. A log plot of D_S^L for the simulation results on pentane versus $1/T$ at $P = 49.89$ atm. The symbols indicate the simulation results from ref 33. The solid line indicates the singular function given by eq 27 with $\eta = 4/3$, where $\kappa = 48$ is a theoretical value for LJ and $T_f = 63.02$ K is a fitting value.

In Figure 8, the volume fraction ϕ dependence of the long-time self-diffusion coefficient D_S^L for the simulation results on hard spheres with 15% size polydispersity is shown. All of the simulation results are well described by eq 12, except in a glass state. This was already shown in Figure 2. The pressure P is calculated for hard spheres by[23]

$$\frac{PV}{Nk_BT} = 1 - \frac{2}{3Nk_BT\Delta t}\sum_{\text{collisions}}\frac{m_i m_j}{m_i + m_j}(\mathbf{V}_i - \mathbf{V}_j)\cdot(\mathbf{X}_i - \mathbf{X}_j) \quad (30)$$

where the summation is taken over all of the collisions that occurred in an appropriate unit time Δt, $\mathbf{V}_i$ is the velocity of ith particle, $\mathbf{X}_i$ is the position vector of ith particle, and m_i is the mass of ith particle. In Figure 9, P is plotted as a function of ϕ. As discussed in the previous paper,[23] one can then find the pressure dependence of D_S^L. In Figure 10, D_S^L is plotted versus P. Then, the simulation results are also well described by eq 27 with $\eta = 4/3$. Thus, the intensive parameter dependence of D_S^L for hard spheres with 15% size polydispersity is shown to be the same as that in fragile liquids. This is consistent with the two facts mentioned above. Hence, this suggests that D_S^L is described by the singular function eq 12 when λ is an extensive parameter, while it is described by the singular function eq 27 when λ is an intensive parameter. In order to check whether this is true for the other systems, we analyze the simulation results on pentane performed by the *NPT* method.[33] In Figure 11, the temperature T dependence of the long-time self-diffusion coefficient D_S^L for the simulation results on pentane is shown at $P = 49.89$ atm. The simulation results from ref 33 are well described by eq 27 with $\eta = 4/3$ within error. The simulation results for the specific volume V from ref 33 are also plotted as a function of temperature T in Figure 12. By using this extensive—intensive relation between V and T, one can also plot the simulation results for D_S^L versus an inverse specific volume $1/V$ in Figure 13. Thus, the simulation results are shown to be well described by eq 12. This situation is exactly the same as that in hard spheres. Hence, there exist two types of master curves in fragile liquids, depending on whether the control parameter is intensive or extensive. This is also true for the EAM-based simulation results performed by the *NPT* method. One of such examples is given by the simulation results for liquid copper at 0 atm.[34] In fact, one can obtain figures similar to Figures 11—13. In Figure 14, we also plot those simulation results as a function of the reduced parameter λ/λ_f together with others, where λ_f is given by λ_c for an extensive parameter. All of the simulation results are well described by eq 12 or eq 29 within error, depending on whether λ is extensive or intensive, respectively. Although there are no data available in strong liquids right now, we conclude that the above suggestion is true for any system, including strong liquids.

5. ANALYSES OF FRAGILE LIQUIDS

Similarly to the previous paper ref 2, we now analyze many experimental data and simulation results for fragile liquids consistently by using eqs 12 and 29, where the control parameter λ is given by inverse temperature $1/T$ here. Thus, we show that eq 29 is a master curve for (F). When the two quantities $\sigma_{\alpha\alpha}\nu_0$ and $\kappa_{\alpha\alpha}$ are known, one can easily obtain the fitting values T_c and T_f by fitting eqs 12 and 29 with various available data, respectively. On the other hand, when those are not known, the singular temperatures and the quantity d_0 must be determined only by fitting.

A. Self-Diffusion of Ni. We first investigate the self-diffusion of Ni, which is contained in different multicomponent metallic melts. In Figure 15, the 10 different experimental data by Meyer et al.[35−41] for the reduced long-time self-diffusion coefficient D_S^L/d_0 are plotted versus T_f/T, where T_f and d_0 are listed in Table 4. All of the data are thus shown to be collapsed onto the master curve given by eq 29 with $\eta = 4/3$. Hence, we assume that all of the data are well described by the master curve as long as the liquids are in equilibrium and start to deviate from it once the liquids become out of equilibrium. Because all of the experimental data of Ni shown here have been observed at rather higher temperatures, such a deviation is not seen for them. At lower temperatures, however, it would be seen in them, as in Figure 17. We note here that the fitting value of d_0 obtained for the experimental data coincides with that obtained by using the Stillinger—Weber (SW) potential.[24] In fact, one can obtain $\kappa_{\text{NiNi}} = 12$ and $\sigma_{\text{NiNi}}\nu_0 = 7.85019 \times 10^{-8}$ m^2/s by using the SW potential. Those lead to $d_0 = 6.542 \times 10^{-9}$ m^2/s. This theoretical value coincides with the fitting value for all of the experimental data within error. Hence, we conclude that this is a characteristic value for Ni, which does not depend on in what kinds of systems Ni is contained. Thus, the SW potential might be suitable to describe the self-diffusion of Ni.

B. Self-Diffusion of Cu. We next investigate the self-diffusion of Cu. In Figure 16, a log plot of D_S^L/d_0 is shown versus T_f/T for Cu in different experiments and simulations. The experiments are for $Al_{90}Cu_{10}$,[42] $Al_{83}Cu_{17}$,[42] $Al_{75}Cu_{25}$,[42] $Al_{80}Cu_{20}$,[43] and Cu_{100},[44] and the simulations are for Cu_{100}[45] and $Cu_{60}Ti_{20}Zr_{20}$.[27,46] All of the data are thus shown to be collapsed onto the master curve given by eq 29 with $\eta = 4/3$, where T_f, T_c, and d_0 are listed in Table 5. The deviation from the master curve is seen in the simulation results for $Cu_{60}Ti_{20}Zr_{20}$ at lower temperatures around $\log_{10}(D_S^L/d_0) \simeq -3.5$, below which those systems are

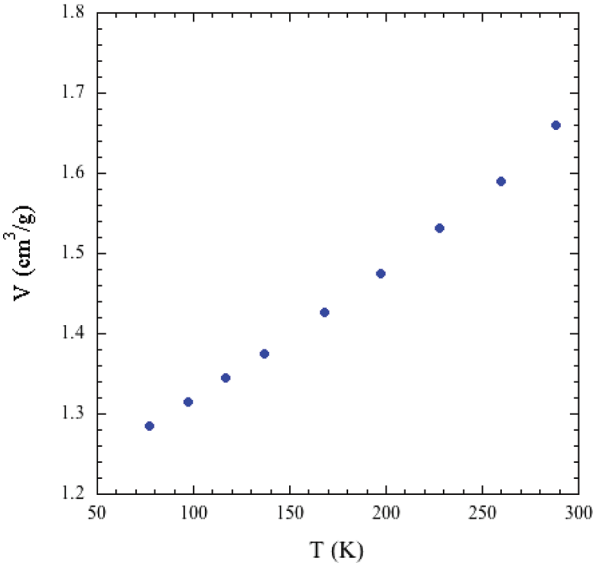

Figure 12. A plot of a specific volume V for the simulation results on pentane versus T at $P = 49.89$ atm. The symbols indicate the simulation results from ref 33.

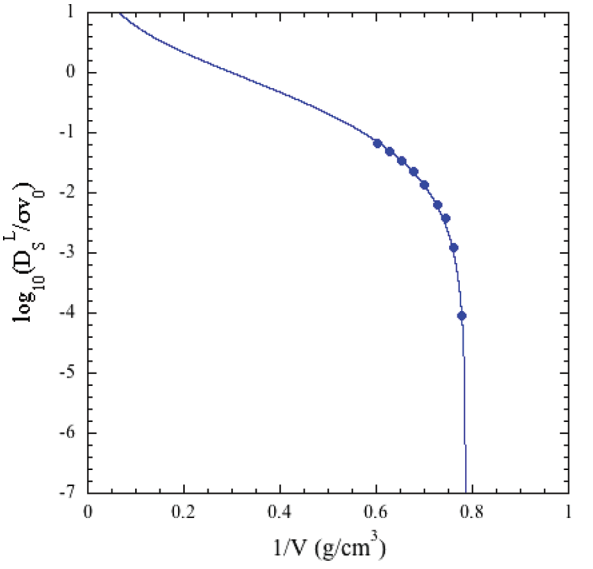

Figure 13. A log plot of D_S^L for the simulation results on pentane versus an inverse specific volume $1/V$ at $P = 49.89$ atm. The symbols indicate the simulation results from ref 33. The solid line indicates the singular function given by eq 12, where $\kappa = 1$ and $V_c = 1.273$ cm^3/g are fitting values.

considered to be out of equilibrium. We note here that the fitting value of d_0 for the simulation results of Cu_{100} coincides with those for the experimental data of Cu_{100} and Al_xCu_{100-x}. Hence, the potential used in those simulations are reasonable to describe the self-diffusion of Cu. However, we should mention that the theoretical value of d_0 obtained by using the HT potential[27] for $Cu_{60}Ti_{20}Zr_{20}$ does not agree with the experimental value, although their reduced values of D_S^L/d_0 are all collapsed onto the master curve $f(x)$ given by eq 29.

C. Self-Diffusion of Metallic Melts. We here investigate the self-diffusion of other metallic melts. In Figure 17, a log plot of

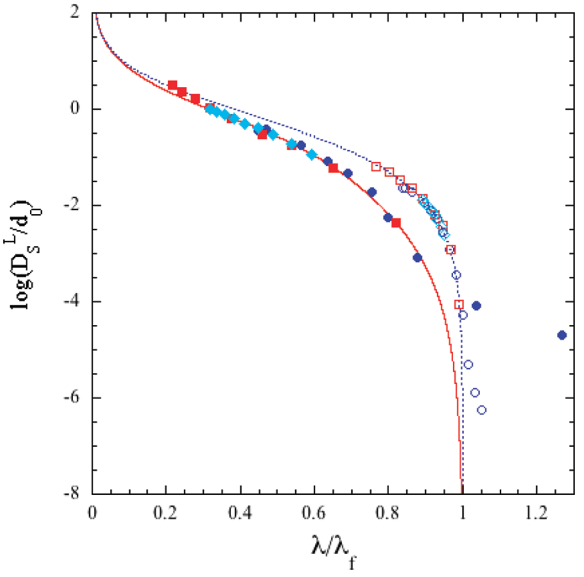

Figure 14. A log plot of D_S^L/d_0 versus λ/λ_f for the simulation results on hard spheres,[23] pentane,[33] and Cu.[34] The open symbols indicate the simulation results for an extensive parameter, and the filled symbols are for an intensive parameter; (○) hard spheres, (□) pentane, and (◊) Cu with the fitting values $T_f = 536$ K and $d_0 = 5.9 \times 10^{-9}$ m^2/s for temperature dependence and also with the fitting values $V_c = 0.117$ cm^3/g and $\kappa = 1$ for volume dependence. The dotted line is the singular function given by eq 12, and the solid line indicates the singular function given by eq 29 with $\eta = 4/3$.

D_S^L/d_0 is shown versus T_f/T for different metals. The experiments are Li in $LiCl/7H_2O$[47] and Ti_{100},[48] and the simulations are Al and Ni in $Al_{80}Ni_{20}$,[49] Ni in $Al_{50}Ni_{50}$,[50] Al in $Al_{50}Ni_{50}$,[50] Ti_{100},[48] Au_{100},[45] and Ni in $Ni_{20}Zr_{80}$,[51] where T_f, T_c, and d_0 are listed in Table 6. All of the data are thus shown to be collapsed onto the master curve given by eq 29 with $\eta = 4/3$. The deviation from the master curve is seen in the simulation results for $LiCl/7H_2O$, $Al_{80}Ni_{20}$, and $Ni_{20}Zr_{80}$ at lower temperatures around $\log_{10}(D_S^L/d_0) \simeq -3.5$, below which those systems are considered to be out of equilibrium. We note here that the fitting value of d_0 for the simulation results of Ti_{100} coincides with that for the experimental data of Ti_{100}.

D. Self-Diffusion of Viscous Liquids. We now investigate the self-diffusion of viscous liquids. We separate liquids into two groups (a) and (b) for convenience; (a) experiments: OTP[52−54] and polyethylene and polystyrene,[55] (a) simulations: OTP[53] and polyethlene and polystyrene;[56] (b) experiments: toluene,[57] salol, PDE, CDE, terracene, TNB, rubrene,[58] and diopside.[59] In Figure 18a and b, a log plot of D_S^L/d_0 is shown versus T_f/T for groups (a) and (b), respectively, where T_f, T_c, and d_0 are listed in Table 7. All of the data for viscous liquids are thus shown to be collapsed onto the master curve given by eq 29 with $\eta = 4/3$. The deviation from the master curve is obviously seen in OTP, toluene, rubrene, diopside, tetracene, and PDE at lower temperatures around $\log_{10}(D_S^L/d_0) \simeq -5.0$, below which those systems are considered to be out of equilibrium.

E. Self-Diffusion of Water. We finally investigate the self-diffusion of water as one of examples in fragile liquids. We discuss the self-diffusion of bulk water and that of confined water separately.

1. Bulk Water. First, we analyze the self-diffusion data of bulk water observed by experiments[60−66] and also by simulations.[60,69] In Figure 19, a log plot of D_S^L/d_0 is shown versus T_f/T for bulk

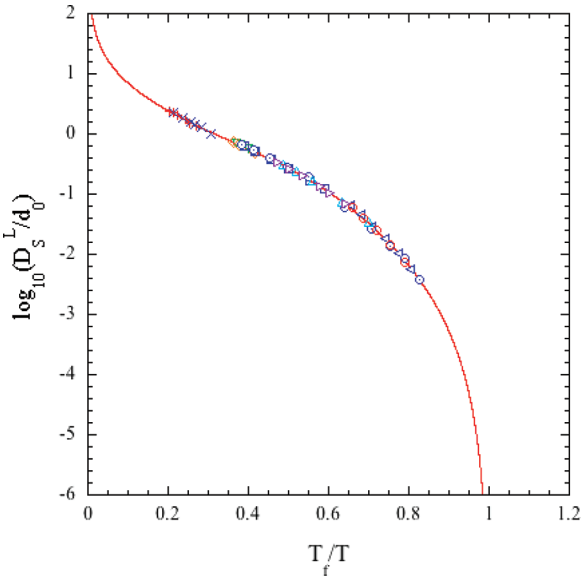

Figure 15. A log plot of the reduced long-time self-diffusion coefficient D_S^L/d_0 of Ni versus T_f/T for the experimental data and the simulation results. The symbols indicate the experimental data and the simulation results for Ni. Experiments: (+) $Si_{90}Ni_{10}$,[35] (×) $Si_{80}Ni_{20}$,[35] (left-pointing triangle) $Pd_{40}Ni_{10}Cu_{30}P_{20}$,[36] (△) $Pd_{40}Ni_{40}P_{20}$,[37] (□) $Ni_{80}P_{20}$,[37] (⊙) $Pd_{43}Ni_{10}Cu_{27}P_{20}$,[38] (◊) $Al_{25}Ni_{75}$,[39] (▽) $Al_{50}Ni_{50}$,[39] (right-pointing triangle) $Zr_{64}Ni_{36}$,[40] and (○) $Zr_{41.2}Ti_{13.8}Cu_{12.5}Ni_{10}Be_{22.5}$.[41] The solid line indicates the master curve given by eq 29 with $\eta = 4/3$. Here T_f, T_c, $\kappa_{\alpha\alpha}$, and d_0 are listed in Table 4.

Table 4. T_f (K), T_c (K), $\kappa_{\alpha\alpha}$, and d_0 (10^{-9} m^2/s) for Ni, where d_0^* Indicates a Theoretical Value

system [ref]	symbol	T_f	T_c	$\kappa_{\alpha\alpha}$	d_0
Experiments					
$Si_{90}Ni_{10}$[35]	(+)	370.3	448.4	12	6.54*
$Si_{80}Ni_{20}$[35]	(×)	389.1	465.1	12	6.54*
$Pd_{40}Ni_{10}Cu_{30}P_{20}$[36]	(left-pointing triangle)	675.7	806.5	12	6.54*
$Pd_{40}Ni_{40}P_{20}$[37]	(△)	675.7	813.0	12	6.54*
$Pd_{43}Ni_{10}Cu_{27}P_{20}$[38]	(⊙)	689.7	826.4	12	6.54*
$Ni_{80}P_{20}$[37]	(□)	699.3	840.3	12	6.54*
$Al_{25}Ni_{75}$[39]	(◊)	704.2	840.3	12	6.54*
$Al_{50}Ni_{50}$[39]	(▽)	704.2	840.3	12	6.54*
$Zr_{64}Ni_{36}$[40]	(right-pointing triangle)	781.3	934.6	12	6.54*
$Zr_{41.2}Ti_{13.8}Cu_{12.5}Ni_{10}Be_{22.5}$[41]	(○)	787.4	934.6	12	6.54*

water, where T_f, T_c, and d_0 are listed in Table 8. For comparison, we also plot the experimental data[67] and the simulation results[70] of hydration water for lysozyme and the experimental data for bulk methanol[68] in Figure 19. All of the data are again shown to be collapsed onto the master curve given by eq 29 with $\eta = 4/3$. The deviation from the master curve is obviously seen in the experiment and the simulation for lysozyme water at lower temperatures around $\log_{10}(D_S^L/d_0) \simeq -4$, below which those liquids are considered to be out of equilibrium.

2. Confined Water. We next analyze the self-diffusion data of confined water observed experimentally by Mallamace et al.[67,71]

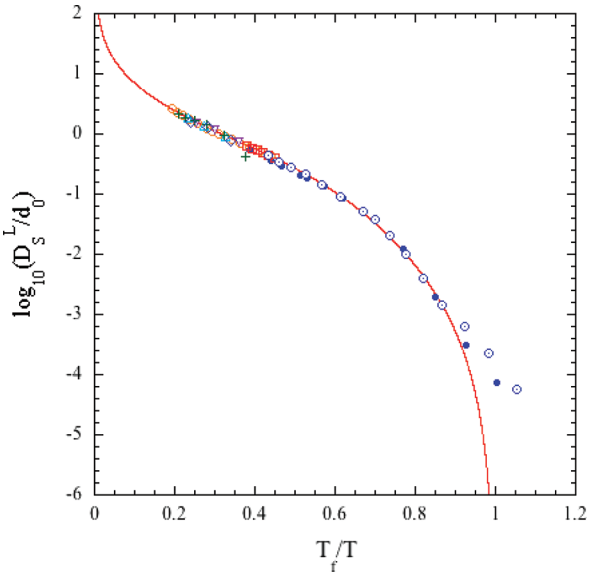

Figure 16. A log plot of D_S^L/d_0 versus T_f/T for Cu. The symbols indicate the experimental data and the simulation results. Experiments: (△) $Al_{90}Cu_{10}$,[42] (◊) $Al_{83}Cu_{17}$,[42] (▽) $Al_{75}Cu_{25}$,[42] (+) $Al_{80}Cu_{20}$,[43] and (□) Cu_{100}.[44] Simulations: (○) Cu_{100},[45] (●) $Cu_{60}Ti_{20}Zr_{20}$,[46] and (⊙) $Cu_{60}Ti_{20}Zr_{20}$.[27] Here, T_f, T_c, $\kappa_{\alpha\alpha}$, and d_0 are listed in Table 5. The details are the same as those in Figure 15.

Table 5. T_f (K), T_c (K), $\kappa_{\alpha\alpha}$, and d_0 (10^{-9} m^2/s) for Cu

system [ref]	symbol	T_f	T_c	$\kappa_{\alpha\alpha}$	d_0
Experiments					
$Al_{90}Cu_{10}$[42]	(△)	319.5	390.6		8.318
$Al_{83}Cu_{17}$[42]	(◊)	331.1	411.5		8.318
$Al_{75}Cu_{25}$[42]	(▽)	350.9	423.7		8.318
$Al_{80}Cu_{20}$[43]	(+)	378.8	454.5		8.318
Cu_{100}[44]	(□)	617.3	740.7		8.318
Simulations					
Cu_{100}[45]	(○)	617.3	740.7		8.318
$Cu_{60}Ti_{20}Zr_{20}$[46]	(●)	734.2	840.3	9	8.56*
$Cu_{60}Ti_{20}Zr_{20}$[27]	(⊙)	740.7	847.7	9	8.56*

In Figure 20, a log plot of D_S^L/d_0 is shown versus T_c/T for confined water, where T_c and d_0 are listed in Table 9. We should mention here that the experimental data for confined water are all described by the mean-field singular curve given by eq 12 as

$$D_S^L/d_0 = (1-x)^2/x \tag{31}$$

where $x = T_c/T$. The deviation from this master curve is obviously seen in all confined waters at lower temperatures around $\log_{10}(D_S^L/d_0) \simeq -3.0$, below which those liquids are considered to be out of equilibrium. For comparison, the experimental data for bulk methanol[68] and for water in a mixture with methanol[71] are also plotted versus T_f/T in Figure 20, where T_f, T_c, and d_0 are listed in Table 9. The experimental data for bulk liquids are described by the master curve given by eq 29 with $\eta = 4/3$. Thus, we conclude that only the two-body correlations play an important role even in a supercooled state

dx.doi.org/10.1021/jp203583u |J. Phys. Chem. B 2011, 115, 14030–14045

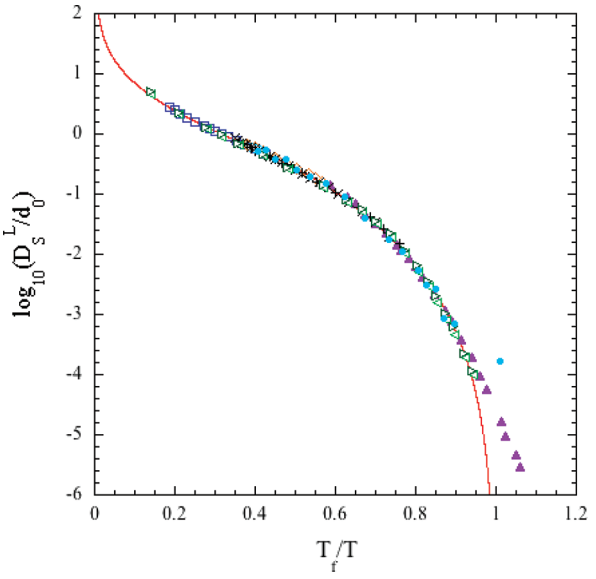

Figure 17. A log plot of D_S^L/d_0 versus T_f/T for metallic melts. The symbols indicate the experimental data and the simulation results. Experiments: (Δ) Li in $LiCl/7H_2O$[47] and (⊙) Ti_{100}.[48] Simulations: (□) Au_{100},[45] (◊) Ti_{100},[48] (right-pointing triangle) Ni in $Al_{80}Ni_{20}$,[49] (left-pointing triangle) Al in $Al_{80}Ni_{20}$,[49] (×) Ni in $Al_{50}Ni_{50}$,[50] (+) Al in $Al_{50}Ni_{50}$,[50] and (●) Ni in $Ni_{20}Zr_{80}$.[51] Here, T_f, T_c, $\kappa_{\alpha\alpha}$, and d_0 are listed in Table 6. The details are the same as those in Figure 15.

Table 6. T_f (K), T_c (K), $\kappa_{\alpha\alpha}$, and d_0 (10^{-9} m^2/s) for Metals

system [ref]	symbol	T_f	T_c	$\kappa_{\alpha\alpha}$	d_0
Experiments					
Li in $LiCl/7H_2O$[47]	(Δ)	184.9	219.8		6.310
Ti_{100}[48]	(⊙)	797.4	947.9		10.00
Simulations					
Au_{100}[45]	(□)	598.8	714.3		6.761
Ni in $Al_{80}Ni_{20}$[49]	(right-pointing triangle)	627.0	743.5		10.72
Al in $Al_{80}Ni_{20}$[49]	(left-pointing triangle)	628.9	769.2		10.96
Ni in $Al_{50}Ni_{50}$[50]	(×)	699.3	847.5		8.00
Al in $Al_{50}Ni_{50}$[50]	(+)	722.0	875.7		7.94
Ti_{100}[48]	(◊)	797.4	947.9		10.00
Ni in $Ni_{20}Zr_{80}$[51]	(●)	807.8	970.9		105.93

[S] for quasi-one- and two-dimensional confined waters, while the many-body correlations start to play an important role in [S] for bulk water. This is a reason why the relaxation times of confined water follow MCT predictions[72] because MCT solutions also obey eq 31 even for an intensive parameter.

6. ANALYSES OF STRONG LIQUIDS

We finally analyze the simulation results for SiO_2 as a typical example of strong liquids. In Figure 21a and b, a log plot of D_S^L/d_0 is shown versus T_f/T for (a) recent simulation results on SiO_2 for different potentials[22,73−77] and (b) old simulation results on O in SiO_2 for different potentials.[76] For comparison, the simulation results for O in $CaAl_2Si_2O_8$[77] are also shown in Figure 21a, where

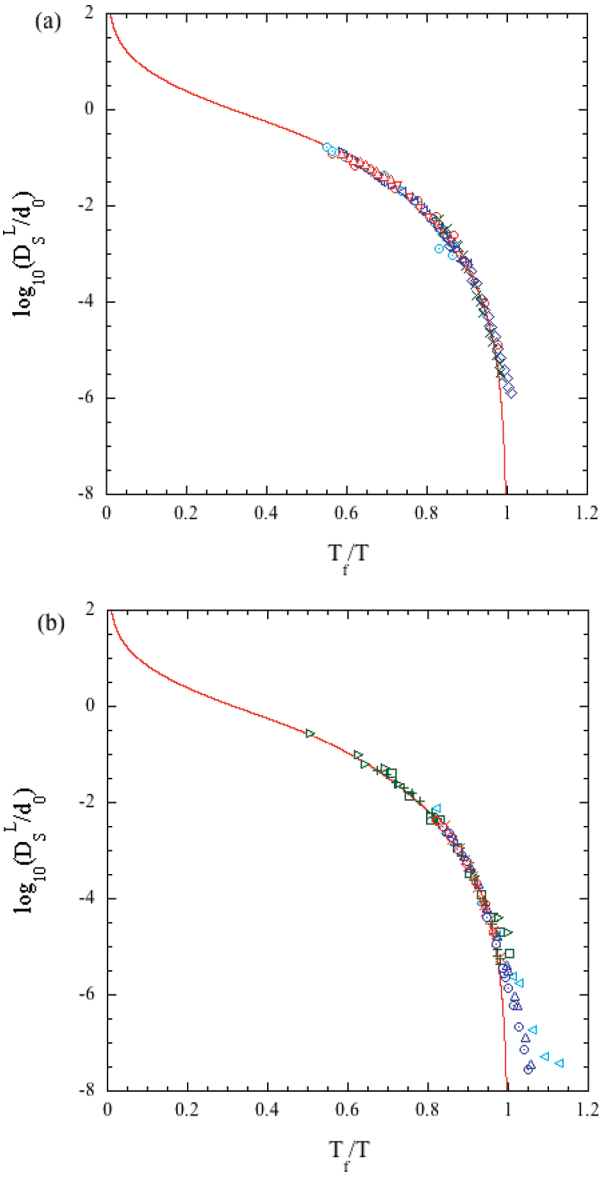

Figure 18. A log plot of D_S^L/d_0 versus T_f/T for viscous liquids. The symbols indicate the experimental data and the simulation results. (a) Experiments: (○) OTP (diffusion),[52] (◊) OTP (NMR),[52] (+) OTP,[53] (×) OTP,[54] (Δ) polyethylene 2440,[55] (▽) polystyrene 2440.[55] Simulations: (⊙) OTP,[53] (right-pointing triangle) polyethylene,[56] and (left-pointing triangle) polystyrene.[56] (b) Experiments: (right-pointing triangle) toluene,[57] (+) salol,[58] (□) PDE,[58] (×) CDE,[58] (Δ) tetracene,[58] (○) TNB,[58] (⊙) rubrene,[58] and (left-pointing triangle) diopside.[59] Here, T_f, T_c, $\kappa_{\alpha\alpha}$, and d_0 are listed in Table 7. The details are the same as those in Figure 15.

$T_f = 2008.0$ K, $T_c = 2561.1$ K, and $d_0 = 14.1 \times 10^{-9}$ m^2/s. Thus, all of the results are shown to be collapsed onto the master curve given by eq 29 with $\eta = 5/3$. Here, the deviation from the master curve starts at lower temperatures around $\log_{10}(D_S^L/d_0) \simeq -3.0$. Hence, we note that the value of D_S^L/d_0, below which the liquids become out of equilibrium, is higher than that in fragile liquids. We should also mention here that the exponent $\eta = 5/3$ is slightly different from $\eta = 4/3$ in fragile liquids. This is mainly considered to result from the long-range nature of interactions between atoms. We discuss this next.

dx.doi.org/10.1021/jp203583u |J. Phys. Chem. B 2011, 115, 14030–14045

Table 7. T_f (K), T_c (K), $\kappa_{\alpha\alpha}$, and d_0 (10^{-9} m^2/s) for Viscous Liquids

system [ref]	symbol	T_f	T_c	$\kappa_{\alpha\alpha}$	d_0
		Liquids (a)			
Experiments					
OTP (diffusion)[52]	(○)	224.2	272.5		10.0
OTP[53]	(+)	274.0	333.3		15.1
OTP[54]	(×)	277.0			10.0
OTP (NMR)[52]	(◇)	282.5			20.9
polyethylene[55]	(Δ)	285.7	341.3		0.631
polystyrene[55]	(▽)	380.2	446.4		1.2
Simulations					
OTP[53]	(⊙)	243.9	294.1		6.31
polyethylene[56]	(right-pointing triangle)	289.9	344.8		0.631
polystyrene[56]	(left-pointing triangle)	386.1	456.6		0.631
		Liquids (b)			
Experiments					
toluene[57]	(right-pointing triangle)	141.2	173.3		8.91
salol[58]	(+)	248.1	298.5		12.6
PDE[58]	(□)	341.3	416.7		15.8
CDE[58]	(×)	363.6	442.5		10.0
terracene[58]	(Δ)	384.6			0.40
TNB[58]	(○)	390.6			0.13
rubrene[58]	(⊙)	392.2			0.20
diopside[59]	(left-pointing triangle)	1369.9	1666.6		8.91

In order to study SiO_2 by the molecular dynamics simulations, several potentials have been proposed.[26,73,74,76,78] Kob[74] has used the BKS potential proposed by van Beest, Kramer, and van Santen[78] as

$$U_{BKS}(r_{ij}) = q_i q_j e^2/r_{ij} + A_{ij}e^{-B_{ij}r_{ij}} - C_{ij}/r_{ij}^6 \quad (32)$$

where the constants A_{ij}, B_{ij}, and C_{ij} are found in ref 78 and e is a charge of an electron. Morgan et al.[77] have also used the potential given by eq 32 with $C_{ij} = 0$ to study $CaAl_2Si_2O_8$. Recently, Carré et al.[73] have proposed an effective potential (called the CHIK potential), which improves the BKS potential, and discussed the dynamics of SiO_2. Voigtmann et al.[75] have used this potential and studied the dynamics of silica melts under higher pressure. Those potentials all contain Coulomb long-range interactions. Then, it is known that those potentials can generate such a tetrahedral network because of a long-range nature, which mimics the three-body interactions.[74]

On the other hand, Nakano et al[26] have proposed the potential (called the NV potential) containing the three-body potential $U^{(3)}(r_{ij})$ in addition to the two-body short-range potential $U^{(2)}(r_{ij})$, which are given by

$$U^{(2)}(r_{\alpha\beta}) = \epsilon_{\alpha\beta}[(a_{\alpha\alpha} + a_{\beta\beta})/r]^{n_{\alpha\beta}} + Z_\alpha Z_\beta e^{-r_{\alpha\beta}/A_0}/r_{ij} - (a_\alpha Z_\beta^2 + a_\beta Z_\alpha^2)e^{-r_{\alpha\beta}/A_1}/(2r_{\alpha\beta}^4) \quad (33)$$

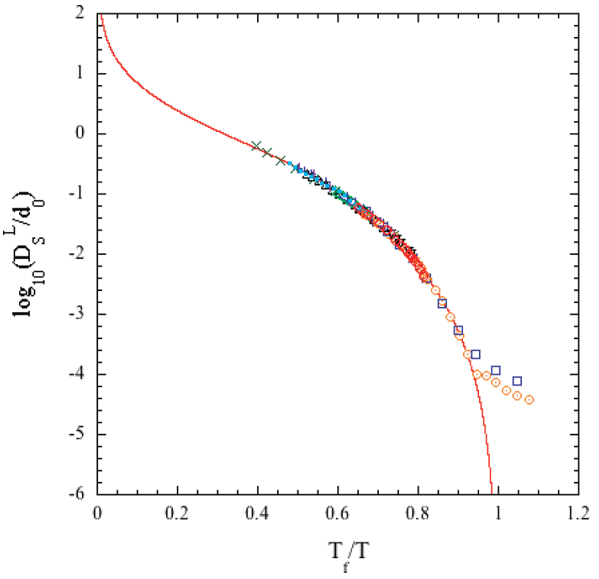

Figure 19. A log plot of D_S^L/d_0 versus T_f/T for bulk water. The symbols indicate the experimental data and the simulation results. Experiments: (|) Krasnenko et al.,[60] (○) Price et al.,[61] (Δ) Easteal et al.,[62] (left-pointing triangle) Mills et al.,[63] (◇) Holz et al.,[64] (right-pointing triangle) Gillen et al.,[65] and (▽) Prielmeier et al.[66] Simulations: (×) Krasnenko et al.[60] and (+) Selvan et al.[69] For comparison, the experimental data[67] and the simulation results[70] of hydration water for lysozyme are also plotted by (⊙) and (□), respectively. The experimental data for bulk methanol[68] are also plotted by (●) for comparison. Here, T_f, T_c, $\kappa_{\alpha\alpha}$, and d_0 are listed in Table 8. The details are the same as those in Figure 15.

Table 8. T_f (K), T_c (K), $\kappa_{\alpha\alpha}$, and d_0 (10^{-9} m^2/s) for Bulk Water

system [ref]	symbol	T_f	T_c	$\kappa_{\alpha\alpha}$	d_0
Experiments					
Krasnenko et al.[60]	(|)	188.7			31.6
Price et al.[61]	(○)	193.8	229.9		38.0
Easteal et al.[62]	(Δ)	195.1	235.3		39.8
Mills et al.[63]	(left-pointing triangle)	195.1	235.3		39.8
Holz et al.[64]	(◇)	195.1	235.3		39.8
Gillen et al.[65]	(right-pointing triangle)	200.0			50.1
Prielmeier et al.[66]	(▽)	200.0			50.1
lysozyme water[67]	(⊙)	215.5			3.72
methanol[68]	(●)	137.0	165.3		5.56
Simulations					
Krasnenko et al.[60]	(×)	148.1			20.0
Selvan et al.[69]	(+)	160.0			20.9
lysozyme water[70]	(□)	210.1			2.51

$$U^{(3)}(r_{\alpha\beta}, r_{\alpha\gamma}) = B_\alpha \exp[(r_{\alpha\beta} - r_0)^{-1} + (r_{\alpha\gamma} - r_0)^{-1}] \times [r_{\alpha\beta}\cdot r_{\alpha\gamma}/(r_{\alpha\beta}r_{\alpha\gamma}) - \cos\theta_\alpha]^2 \times \theta(r_0 - r_{\alpha\beta})\theta(r_0 - r_{\alpha\gamma}) \quad (34)$$

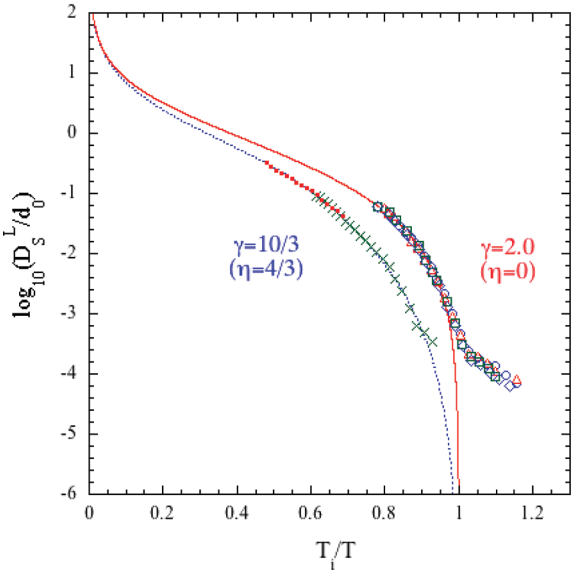

Figure 20. A log plot of D_S^L/d_0 versus T_c/T for confined water. The symbols indicate the experimental data; (Δ) hydration water for lysozyme with hydration level h = 0.3,[67] (○) hydration water for lysozyme with hydration level h = 0.32,[67] (□) a fully hydrated MCM-41-S sample with a pore diameter of 14 Å,[71] and (◊) a fully hydrated MCM-41-S sample with a pore diameter of 18 Å.[71] The solid line indicates the mean-field curve given by eq 31. For comparison, the experimental data for bulk liquids are also shown versus T_f/T; (●) bulk methanol[68] and (×) water in a water−methanol mixture.[71] The dotted line indicates the mater curve given by eq 29 with $\eta = 4/3$. Here, $T_i = T_c$ for confined water and T_f for bulk liquids, where T_f, T_c, and d_0 are listed in Table 9.

Table 9. T_f (K), T_c (K), $\kappa_{\alpha\alpha}$, and d_0 (10^{-9} m^2/s) for Confined Water

system [ref]	symbol	T_f	T_c	$\kappa_{\alpha\alpha}$	d_0
Experiments for Confined Water					
h = 0.3 NMR[67]	(Δ)		230.9		1.78
h = 0.32 NMR[67]	(○)		230.9		1.78
14 Å NMR[71]	(□)		227.3		26.9
18 Å NMR[71]	(◊)		227.3		26.9
Experiments for Bulk Liquids					
methanol[68]	(●)	137.0	165.3		5.56
water in solution[71]	(×)	190.7	227.3		17.4

where $\theta(x)$ is a step function and the potential parameters are found in ref 26. Here, $\sigma_{\alpha\alpha} = 2a_{\alpha\alpha}$ and $v_0 = (\epsilon_{\alpha\alpha}/m_\alpha)^{1/2}$. By using this NV potential, one can now show how the three-body interactions affect the value of the exponent η. In Figure 22, a log plot of D_S^L/d_0 is shown versus T_f/T for the simulation results obtained by the NV potential with and without three-body potential $U^{(3)}(r)$. Then, the simulation results without three-body potential $U^{(3)}(r)$ are shown to be described by the master curve given by eq 29 with $\eta = 4/3$, where T_f, T_c, $\kappa_{\alpha\alpha}$, and d_0 are listed in Table 11. On the other hand, as shown in Figure 21, those with three-body potential $U^{(3)}(r)$ are described by the master curve given by eq 29 with $\eta = 5/3$. Thus, the three-body interactions are shown to slightly change the value of the exponent η from 4/3 to 5/3. Hence, we conclude that the

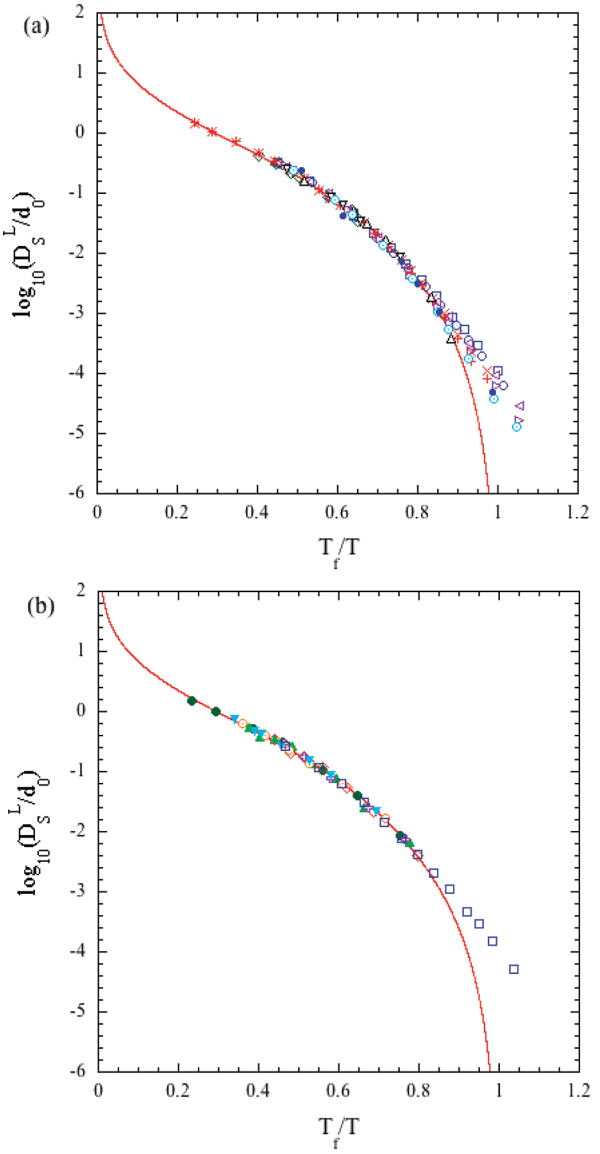

Figure 21. A log plot of D_S^L/d_0 versus T_f/T for SiO_2. The symbols indicate the simulation results for SiO_2; (a) (left-pointing triangle) O in SiO_2,[73] (right-pointing triangle) Si in SiO_2,[73] (×) O in SiO_2,[22] (+) Si in SiO_2,[22] (□) O in SiO_2,[74] (○) Si in SiO_2,[74] (▽) Si in SiO_2 (ρ = 3.3 g/cm^{-3}),[75] (Δ) Si in SiO_2 (ρ = 3.9 g/cm^{-3}),[75] (●) Si in SiO_2 (ρ = 2.7 g/cm^{-3}),[75] (⊙) Si in SiO_2 (ρ = 2.21 g/cm^{-3}),[75] and (◊) O in $CaAl_2Si_2O_8$.[77] (b) O in SiO_2 for different potentials;[76] (○) Modified Mastui, (Δ) Tsuneyuki, (◊) BKS, (⊙) TRIM, (+) Kubicki, (▽) Poole, and (□) Horbach (BKS).The solid line indicates the master curve given by eq 29 with $\eta = 5/3$, where T_f, T_c, $\kappa_{\alpha\alpha}$, and d_0 are listed in Table 10.

main difference between (S) and (F) results from an interaction range of pair potentials. Thus, the Coulomb long-range interactions are shown to mimic the three-body interactions and lead to strong liquids (see Figure 21). Finally, we mention that, as shown in Table 11, d_0 and $\kappa_{\alpha\alpha}$ do not depend on $U^{(3)}(r)$, while T_i does.

7. SUMMARY

In the present paper, we have fully analyzed the experimental data and the simulation results for the long-time self-diffusion

Table 10. T_f (K), T_c (K), $\kappa_{\alpha\alpha}$, and d_0 (10^{-9} m^2/s) for Strong Liquids

system [ref]	symbol	T_f	T_c	$\kappa_{\alpha\alpha}$	d_0
(a) Simulations for SiO_2					
O in SiO_2 (CHIK)[73]	(left-pointing triangle)	2369.7	2994.0		45.7
Si in SiO_2 (CHIK)[73]	(right-pointing triangle)	2381.0	2994.0		36.2
O in SiO_2 (NV)[22]	(×)	2418.0	3087.0	15.31	49.1*
Si in SiO_2 (NV)[22]	(+)	2427.5	3097.3	27.35	37.1*
O in SiO_2 (BKS)[74]	(□)	2762.4	3496.5		28.8
Si in SiO_2 (BKS)[74]	(○)	2793.3	3546.1		24.0
Si in SiO_2 (CHIK, 3.30)[75]	(▽)	1686.3	2136.8		11.0
Si in SiO_2 (CHIK, 3.90)[75]	(△)	1851.9	2283.1		12.6
Si in SiO_2 (CHIK, 2.70)[75]	(●)	2193.0	2762.4		35.5
Si in SiO_2 (CHIK, 2.21)[75]	(⊙)	2544.5	3205.1		43.7
(b) Simulations for O in SiO_2					
modified Mastui[76]	(○)	2293.6	2941.2		52.9
Tsuneyuki[76]	(△)	2638.5	3448.3		63.1
Horbach (BKS)[76]	(□)	2890.2	3703.7		63.1
BKS[76]	(◇)	3048.8	3906.3		66.1
Poole[76]	(▽)	4149.4	5376.3		72.8
TRIM[76]	(⊙)	4184.1	5376.3		64.9
Kubicki[76]	(+)	4545.5	5882.4		97.7

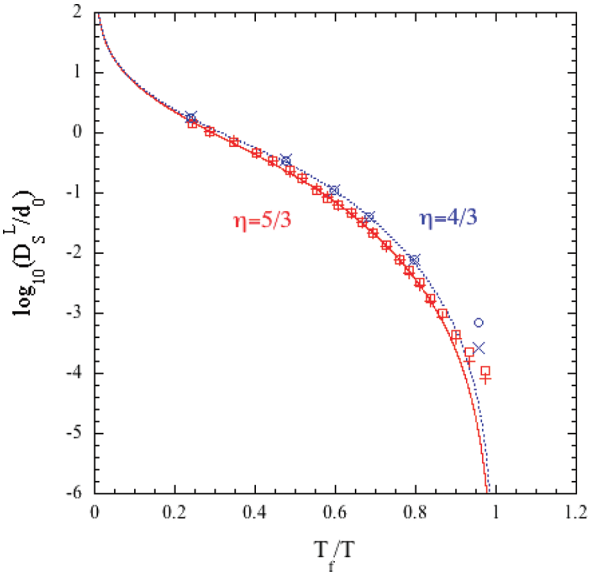

Figure 22. A log plot of the reduced long-time self-diffusion coefficient D_S^L/d_0 versus T_f/T for SiO_2. The symbols indicate the simulation results for SiO_2; (□) O in SiO_2 for the NV potential with three-body potential $U^{(3)}(r)$,[22] (+) Si in SiO_2 for the NV potential with three-body potential $U^{(3)}(r)$,[22] (○) O in SiO_2 for the NV potential without three-body potential $U^{(3)}(r)$,[22] and (×) Si in SiO_2 for the NV potential without three-body potential $U^{(3)}(r)$.[22] The solid line indicates the master curve given by eq 29 with $\eta = 5/3$, while the dotted line is from eq 29 with $\eta = 4/3$, where T_f, T_c, $\kappa_{\alpha\alpha}$, and d_0 are listed in Table 11.

coefficient D_S^L in four different types of glass-forming liquids from a unified point of view recently proposed by the present author,[1,2] (F) fragile liquids, (S) strong liquids, (CW) confined waters, and (O) other glass formers. Typical examples of (F) are metallic melts, viscous liquids, and bulk water, while those of (S) are SiO_2 with different potentials. Then, we showed that there exist two types of master curves in (F) and (S), depending on whether the control parameter is intensive or extensive. For an extensive parameter, the master curve is given by the singular function eq 12, while for an intensive parameter, it is given by the singular function eq 29. All of the self-diffusion data for different atoms contained in (F) and (S) are collapsed on each master curve, depending on a type of λ. On the other hand, the diffusion data in (CW) and (O) are described by eq 12, irrespective of the type of λ. Thus, we conclude that in a supercooled state of (F) and (S), the many-body correlations play an important role because $\eta \neq 0$, while in (CW) and (O), only the two-body correlations play a role because $\eta = 0$ even for an intensive parameter. We have also shown that the difference between $\eta = 4/3$ in (F) and $\eta = 5/3$ in (S) results from how long the interaction range between atoms is, a short-range or a long-range. Hence, we emphasize that the intensive parameter dependence of the long-time self-diffusion coefficient can provide us more useful information to study a supercooled state. Through the analyses of available data, we have shown that as long as the liquids are in equilibrium, any self-diffusion data can be described

Table 11. T_f (K), T_c (K), $\kappa_{\alpha\alpha}$, and d_0 (10^{-9} m^2/s) for the NV Potential

system [ref]	symbol	T_f	T_c	$\kappa_{\alpha\alpha}$	d_0
Simulations without $U^{(3)}(r)$					
O in SiO_2 (NV)[22]	(○)	2374.6	2857.1	15.31	49.1*
Si in SiO_2 (NV)[22]	(×)	2386.5	2873.6	27.35	37.1*
Simulations with $U^{(3)}(r)$					
O in SiO_2 (NV)[22]	(×)	2418.0	3087.0	15.31	49.1*
Si in SiO_2 (NV)[22]	(+)	2427.5	3097.3	27.35	37.1*

Table 12. Value of $\log_{10}(D_S^L/d_0)$ at Which the Deviation Starts

system	$\log_{10}(D_S^L/d_0)$	η
(F) Fragile Liquids		
viscous liquids	$\simeq -5.0$	4/3
bulk water	$\simeq -4.0$	4/3
metallic melts	$\simeq -3.5$	4/3
(S) Strong Liquids		
SiO_2	$\simeq -3.0$	5/3
(CW) Confined Water		
confined water	$\simeq -3.0$	0
(HS) Hard Spheres		
colloids (6%)	$\simeq -5.1$	0
hard spheres (6%)	$\simeq -5.1$	0
hard spheres (15%)	$\simeq -5.1$	0
(MCT) MCT Solutions		
quasi-hard spheres (n = 36, 10%)	$\simeq -\infty$	0
LJ binary colloids $A_{80}B_{20}$	$\simeq -\infty$	0

by each master curve, eq 12 or 29, depending on an extensive parameter or an intensive one, respectively, while they start to deviate from it when the liquids become out of equilibrium, leading to a glass state. In Table 12, we list the appropriate values of $\log_{10}(D_S^L/d_0)$ for different types of liquids, at which the deviation from the master curve starts. It seems that those values become larger as the interactions become more complex. Finally, in the present paper, we have proposed the phenomenological theory to describe the self-diffusion processes from a liquid state to a supercooled state and then found the master curve $f(x)$ for an intensive parameter. Hence, the next task is to calculate $f(x)$ analytically from a first principle. In order to achieve this, one needs a new idea to deal with many-body correlations consistently. This will be discussed elsewhere.

■ ACKNOWLEDGMENT

The author is grateful to P. Gallo, M. Imai, F. Mallamace, M. Medina-Noyola, A. Meyer, and S. N. Yannopoulos for fruitful discussions and valuable comments. This work was partially supported by the World Premier International Research Center Initiative, MEXT, Japan ,and also by the Institute of Fluid Science, Tohoku University.

■ REFERENCES

(1) Tokuyama, M. *Phys. Rev. E* **2009**, *80*, 031503.
(2) Tokuyama, M. *Phys. Rev. E* **2010**, *82*, 041501.
(3) Turnbull, D. *Contemp. Phys.* **1969**, *10*, 473.
(4) Angell, C. A. *J. Non-Cryst. Solids* **1991**, *13*, 131.
(5) Ediger, M. D.; Angell, C. A.; Nagel, S. R. *J. Phys. Chem.* **1996**, *100*, 13200.
(6) Debenedetti, P. G.; Stillinger, F. H. *Nature* **2001**, *410*, 259.
(7) Angell, C. A.; Ngai, K. L.; McKenna, G. B.; McMillan, P. F.; Martin, S. W. *J. Appl. Phys.* **2000**, *88*, 3113.
(8) Yeomans-Reyna, L.; Medina-Noyola, M. *Phys. Rev. E* **2001**, *64*, 066114.
(9) Ngai, K. L., Ed. Proceedings of the 4th International Discussion Meeting on Relaxation in fragile Systems. *J. Non-Cryst. Solids* **2002** *307*−*310*.
(10) *Proceedings of the 3rd Int. Symposium on Slow Dynamics in Complex Systems*; Tokuyama, M., Oppenheim, I., Eds.; AIP: New York, 2004; Conf. Proc. 708.
(11) Binder, K.; Kob, W. *Glassy Materials and Disordered Solids*; World Scientific: Singapore, 2005.
(12) Götze, W. *Complex Dynamics of Glass-Forming Liquids*; Oxford University Press: New York, 2009.
(13) (a) Tokuyama, M.; Oppenheim, I. *Phys. Rev E* **1994**, *50*, R16. (b) Tokuyama, M.; Oppenheim, I. *Physica A* **1995**, *216*, 85.
(14) Tokuyama, M. *Physica A* **2009**, *388*, 3083.
(15) Tokuyama, M. *Physica A* **2006**, *364*, 23.
(16) Kubo, R. *J. Math. Phys.* **1963**, *4*, 174.
(17) Rahman, A.; Singwi, K. S.; Sjölander, A. *Phys. Rev.* **1962**, *126*, 986.
(18) Tokuyama, M. *Phys. Rev. E* **2000**, *62*, R5915.
(19) Tokuyama, M. *Physica A* **2007**, *378*, 157.
(20) Narumi, T.; Tokuyama, M. *Rep. Inst. Fluid Science* **2007**, *19*, 73.
(21) Narumi, T.; Tokuyama, M. *Phys. Rev. E* **2011**, to be submitted.
(22) Sasaki, I. Master's Thesis, Tohoku University, 2008.
(23) Tokuyama, M.; Narumi, T.; Kohira, E. *Physica A* **2007**, *385*, 439.
(24) Weber, T. A.; Stillinger, F. H. *Phys. Rev. B* **1985**, *31*, 1954.
(25) Kob, W.; Andersen, H. C. *Phys. Rev. E* **1995**, *52*, 4134.
(26) Nakano, A.; Bi, L.; Kalia, R. K.; Vashishta, P. *Phys. Rev. B* **1994**, *49*, 9441.
(27) Han, X. J.; Teichler, H. *Phys. Rev. E* **2007**, *75*, 061501.
(28) Voigtmann, Th.; Puertas, A. M.; Fuchs, M. *Phys. Rev. E* **2004**, *70*, 061506.
(29) Flenner, E.; Szamel, G. *Phys. Rev. E* **2005**, *72*, 031508.
(30) Tokuyama, M. *AIP Conf. Proc.* **2008**, *982*, 3.
(31) Tokuyama, M. *J. Non-Cryst. Solids* **2011**, *357*, 293.
(32) van Megen, W.; Mortensen, T. C.; Williams, S. R.; Müller, J. *Phys. Rev. E* **1998**, *58*, 6073.
(33) Martín-Betancourt, M.; Roemro-Enrique, J. M.; Rull, L. F. *Mol. Simul.* **2009**, *35*, 1043.
(34) Han, X. J.; Chen, M.; Lü, Y. J. *Int. J. Thermophys.* **2008**, *29*, 1408.
(35) Pommrich, A. I.; Meyer,1, A.; Holland-Moritz, D.; Unruh, T. *Appl. Phys. Lett.* **2008**, *92*, 241922.
(36) Meyer, A.; Busch, R.; Schober, H. *Phys. Rev. Lett.* **1999**, *83*, 5027.
(37) Mavila Chathoth, S.; Meyer, A. *Appl. Phys. Lett.* **2004**, *85*, 4881.
(38) Meyer, A. *Phys. Rev. B* **2002**, *66*, 134205.
(39) Stüber, S; Holland-Moritz, D; Unruh, T.; Meyer, A. *Phys. Rev. B* **2010**, *81*, 024204.
(40) Holland-Moritz, D.; Stüber, S.; Hartmann, H.; Unruh, T.; Hansen, T.; Meyer, A. *Phys. Rev. B* **2009**, *79*, 064204.
(41) Meyer, A.; Petry, W.; Koza, M.; Macht, M.-P. *Appl. Phys. Lett.* **2003**, *83*, 3894.
(42) Dahlborg, U.; Besser, M.; Calvo-Dahlborg, M.; Janssen, S.; Juranyi, F.; Kramer, M. J.; Morris, J. R.; Sordelet, D. J. *J. Non-Cryst. Solids* **2007**, *353*, 3295.
(43) Zhang, B.; Griesche, A.; Meyer, A. *Phys. Rev. Lett.* **2010**, *104*, 035902.
(44) Meyer, A. *Phys. Rev. B* **2010**, *81*, 012102.
(45) Szpunar, B.; Smith, R. W. *J. Phys.: Condens. Matter* **2010**, *22*, 035105.
(46) Fujii, H.; Tokuyama, M. *Phys. Rev. E* **2011**, *83*, 021502.
(47) Feiweier, T.; Isfort, O.; Geil, B.; Fujara, F.; Weingärtner, H. *J. Chem. Phys.* **1996**, *105*, 5737.
(48) Horbach, J.; Rozas, R. E.; Unruh, T.; Meyer, A. *Phys. Rev. B* **2009**, *80*, 212203.
(49) Horbach, J.; Das, S. K.; Griesche, A.; Macht, M.-P.; Frohberg, G.; Meyer, A. *Phys. Rev. B* **2007**, *75*, 174304.
(50) Levchenko, E. V.; Evteev, A. V.; Beck, D. R.; Belova, I. V.; Murch, G. E. *Comput. Mater. Sci.* **2010**, *50*, 465.
(51) Mutiara, A. B.; Teichler, H. *Phys. Rev. E* **2001**, *64*, 046133.
(52) MaCall, D. W.; Douglss, D. C.; Falcone, D. R. *J. Chem. Phys.* **1969**, *50*, 3839.
(53) Mossa, S.; Di Leonardo, R.; Ruocco, G.; Sampoli, M. *Phys. Rev. E* **2000**, *62*, 612.
(54) Mapes, M. K.; Swallen, S. F.; Ediger, M. D. *J. Phys. Chem. B* **2006**, *110*, 507.
(55) Bachus, R.; Kimmich, R. *Polymer* **1983**, *24*, 964.
(56) Sabbagh, H.; Eu, B. C. *Physica A* **2010**, *389*, 2325.
(57) Hinze, G.; Sillescu, H. *J. Chem. Phys.* **1996**, *104*, 314.
(58) Chang, I.; Sillescu, H. *J. Phys. Chem. B* **1997**, *101*, 8794.
(59) Nascimento, M. L. F.; Ferreira, E. B.; Zanotto, E. D. *J. Chem. Phys.* **2004**, *121*, 8924.
(60) Krasnenko, V.; Tkaczyk, A. H.; Tkaczyk, E. R.; Mauring, K. *Biopolymers* **2008**, *89*, 1136.
(61) Price, S. W.; Hiroyudi, I.; Arata, Y. *J. Phys. Chem. A* **1999**, *103*, 448.
(62) Easteal, A. J.; Price, W. E.; Woolf, L. A. *J. Chem. Soc., Faraday Trans. 1* **1989**, *85*, 1091.
(63) Mills, R. *J. Phys. Chem.* **1973**, *77*, 685.
(64) Holz, M.; Heil, S. R.; Sacco, A. *Phys. Chem. Chem. Phys.* **2000**, *2*, 4740.
(65) Gillen, K. T.; Douglas, D. C.; Hoch, M. J. R. *J. Chem. Phys.* **1972**, *57*, 5117.
(66) Prielmeier, F. X.; Lang, E. W.; Speedy, R. J.; Lüdemann, H. D. *Ber. Bunsen-Ges. Phys. Chem.* **1988**, *92*, 1111.
(67) Mallamace, F.; Chen, S.-H.; Broccio, M.; Corsaro, C.; Crupi, V.; Majolino, D.; Venuti, V.; Baglioni, P.; Fratini, E.; Vannucci, C.; Stanley, H. E. *J. Chem. Phys.* **2007**, *127*, 045104.

(68) Karger, N.; Vardag, T.; Lüdemann, H.-D. *J. Chem. Phys.* **1990**, *93*, 3437.
(69) Selvan, M. E.; Keffer, D. J.; Cui, S.; Paddison, S. J. *J. Phys. Chem. C* **2010**, *114*, 11965.
(70) Lagi, M.; Chu, X.; Kim, C.; Mallamace, F.; Baglioni, P.; Chen, S.-H. *J. Phys. Chem B* **2008**, *112*, 1571.
(71) Mallamace, F.; Branca, C.; Corsaro, C.; Leone, N.; Spooren, J.; Chen, S.-H.; Stanley, H. E.; Chen, S.-H. *J. Phys. Chem. B* **2010**, *114*, 1870.
(72) Gallo, P.; Rovere, M.; Chen, S.-H. *J. Phys. Chem. Lett.* **2010**, *1*, 729.
(73) Carré, A.; Horbach, J.; Ispas, S.; Kob, W. *Europhys. Lett.* **2008**, *82*, 17001.
(74) Kob, W. *J. Phys.: Condens. Matter* **1999**, *11*, R85.
(75) Voigtmann, Th.; Horbach, J. *J. Phys.: Condens. Matter* **2008**, *20*, 244117.
(76) Hemmati, M.; Angell, C. A. In *Physics meets geology*; Aoki, H., Hemley, R., Eds.; Cambridge University Press: New York, 1998.
(77) Morgan, N. A.; Spera, F. J. *Geochim. Cosmochim. Acta* **2001**, *65*, 4019.
(78) van Beest, B. W. H.; Kramer, G. J.; van Santen, R. A. *Phys. Rev. Lett.* **1990**, *64*, 1955.